1989-12

Identification of thermospheric dayglow spectrum for the MUSTANG experiment

Danczyk, Gary Michael

Monterey, California. Naval Postgraduate School

NAVAL POSTGRADUATE SCHOOL
Monterey, California

THESIS

Identification of Thermospheric Dayglow Emissions for the MUSTANG Experiment

by

Gary Michael Danczyk

December 1989

Thesis Advisor: David D. Cleary

Approved for public release; distribution is unlimited.

REPORT DOCUMENTATION PAGE

a. REPORT SECURITY CLASSIFICATION: UNCLASSIFIED	1b RESTRICTIVE MARKINGS
a SECURITY CLASSIFICATION AUTHORITY	3 DISTRIBUTION/AVAILABILITY OF REPORT: Approved for public release; distribution is unlimited.
b DECLASSIFICATION/DOWNGRADING SCHEDULE	
PERFORMING ORGANIZATION REPORT NUMBER(S)	5 MONITORING ORGANIZATION REPORT NUMBER(S)
a NAME OF PERFORMING ORGANIZATION: Naval Postgraduate School; 6a OFFICE SYMBOL (If applicable): 33	7a NAME OF MONITORING ORGANIZATION: Naval Postgraduate School
c. ADDRESS (City, State, and ZIP Code): Monterey, CA 93943–5000	7b. ADDRESS (City, State, and ZIP Code): Monterey, CA 93943–5000
a NAME OF FUNDING/SPONSORING ORGANIZATION; 8b OFFICE SYMBOL (If applicable)	9 PROCUREMENT INSTRUMENT IDENTIFICATION NUMBER
c. ADDRESS (City, State, and ZIP Code)	10 SOURCE OF FUNDING NUMBERS: PROGRAM ELEMENT NO; PROJECT NO; TASK NO; WORK UNIT ACCESSION NO

TITLE (Include Security Classification): IDENTIFICATION OF THERMOSPHERIC DAYGLOW EMISSIONS FOR THE MUSTANG EXPERIMENT

PERSONAL AUTHOR(S): Danczyk, Gary M.

a. TYPE OF REPORT	13b TIME COVERED	14 DATE OF REPORT (Year, Month, Day)	15 PAGE COUNT
Master's Thesis	FROM _____ TO _____	December 1989	105

SUPPLEMENTARY NOTATION: The views expressed in this thesis are those of the author and do not reflect the official policy or position of the Department of Defense or the U.S. Government

COSATI CODES		
FIELD	GROUP	SUB-GROUP

18 SUBJECT TERMS (Continue on reverse if necessary and identify by block number): N_2, O_2, NO, O; Thermosphere; Airglow; MUSTANG experiment; Molecular Spectroscopy

ABSTRACT (Continue on reverse if necessary and identify by block number)

Thermospheric airglow emissions in the wavelength range of 1800 Å to 3400Å, and altitude range of 100 to 330 km were identified. These emissions compose the preliminary data analysis for the Naval Post Graduate School MUSTANG rocket experiment, scheduled for launch from White Sands, New Mexico in February of 1990. Identification of emissions in the wavelength range of the MUSTANG experiment was accomplished using experimental results to support calculated emission feature intensity. All emission features that will contribute to the experimental spectra, as well as those features that will be distinguishable have been tentatively identified. These results confirm the contention that the instrument wavelength range allows observation of major midultraviolet airglow emission bands. The extended wavelength and altitude range for this experiment allows a unique experimental opportunity to observe all major neutral atmospheric constituents in one spectrum. The primary emission band systems that will be

DISTRIBUTION/AVAILABILITY OF ABSTRACT: ☐ UNCLASSIFIED/UNLIMITED ☒ SAME AS RPT ☐ DTIC USERS	21. ABSTRACT SECURITY CLASSIFICATION: UNCLASSIFIED
1. NAME OF RESPONSIBLE INDIVIDUAL: David D. Cleary	22b TELEPHONE (Include Area Code): (408) 646–2828; 22c. OFFICE SYMBOL: 61–Cl

FORM 1473, 84 MAR — 83 APR edition may be used until exhausted. All other editions are obsolete.

SECURITY CLASSIFICATION OF THIS PAGE

UNCLASSIFIED

[19] Continued:

observed are the N_2 Lyman-Birge -Hopfield bands, the O_2 Schumann-Runge bands, the NO Gamma bands and the O 2972Å line. Secondary contributions will be observed from the N_2 Vegard-Kaplan and 2nd Positive bands, the O_2 Herzberg bands, and the NO Epsilon and Delta bands. These combined spectra will insure the MUSTANG experimental goal of measuring N_2 and NO densities, and determining EUV and photoelectron fluxes can be met.

Approved for public release; distribution is unlimited.

Identification of Thermospheric Dayglow Spectrum for the MUSTANG Experiment

by

Gary Michael Danczyk
Captain, United States Army
B.S., United States Military Academy, 1979

Submitted in partial fulfillment of the requirements for
the degree of

MASTER OF SCIENCE IN PHYSICS

from the

NAVAL POSTGRADUATE SCHOOL
December, 1989

ABSTRACT

Thermospheric airglow emissions in the wavelength range of 1800 Å to 3400Å and altitude range of 100 to 330 km were identified. These emissions compose the preliminary data analysis for the Naval Post Graduate School MUSTANG rocket experiment scheduled for launch from White Sands, New Mexico in February of 1990. Identification of emissions in the wavelength range of the MUSTANG experiment was accomplished using experimental results to support calculated emission intensities. All emission bands that will contribute to the experimental spectra, as well as those features that will be distinguishable, have been tentatively identified. These results confirm the contention that the instrument wavelength range allows observation of the major midultraviolet airglow emission bands. The extended wavelength and altitude range for this experiment allows a unique experimental opportunity to observe all major neutral atmospheric constituents in one spectrum. The primary emission band systems that will be observed are the N_2 Lyman-Birge -Hopfield bands, the O_2 Schumann-Runge bands, the NO Gamma bands and the O 2972Å line. Secondary contributions will be observed from the N_2 Vegard-Kaplan and 2nd Positive bands, the O_2 Herzberg bands, and the NO Epsilon and Delta bands. These combined spectra will insure that the MUSTANG experimental goal of measuring N_2 and NO densities and determining EUV and photoelectron fluxes can be met.

TABLE OF CONTENTS

LIST OF TABLES

LIST OF FIGURES

I. INTRODUCTION

There are many factors motivating the investigation of ionospheric photochemistry. The Department of Defense has several areas of interest in this field. A 1986 Joint Chiefs of Staff memorandum identified fifty critical geophysical parameters that need to be determined. The determination of electron density was ranked fifth on the list (MJCS, 1986). The DoD's concern in furthering the understanding of the ionosphere is based on three known needs:

- Measure the ionosphere for over the horizon radar applications.
- Measure the ionosphere for uni-directional communications.
- SDI beam weapons require identification of low absorption windows for propagation in the upper atmosphere.

Additionally, there is a purely scientific interest in fully identifying physical processes in the upper atmosphere.

These motivating factors have led to the Naval Post Graduate School rocket experiment called MUSTANG. The mission of this experiment is to investigate ionospheric photochemistry. Three specific experimental goals have been established. These are:

- measure NO density in the E-region ionosphere.
- measure N_2 density in the E-, F1, F2 regions.
- infer solar EUV flux and photoelectron flux.

This is a joint rocket experiment containing two ultra-violet spectographs. The Naval Post Graduate School is responsible for a spectograph measuring ultraviolet radiation from 1800 angstroms (Å) down to 3400Å. The Naval Research Laboratory is responsible for a spectograph measuring from 500Å down to 1500Å. The launch vehicle is a Black-Brandt sounding rocket, which is scheduled for a February, 1990 launch date at White Sands, New Mexico. NASA is responsible for the launch. Observations will be made from 100 to 330 km in altitude.

A. THESIS GOALS

The primary objective for this thesis is to identify emission band systems with features between 1800 and 3400 Å in wavelength, that are observable from 100 to 330 km in altitude. The accomplishment of this thesis objective will assist in verifying that the MUSTANG experimental goals are attainable.

B. THESIS OUTLINE

Chapters II through V lead to the identification of those atmospheric constituents with emission features in the 1800-3400 Å range. Chapter II describes the experimental environment which is the ionosphere between 100 and 400 km. Chapter III describes the general physical process that are the principal methods of transferring solar flux energy to create the ionosphere and airglow. Chapter IV describes two facets of molecular spectroscopy. The first of these is molecular transitions. The second is synthetic spectra. Chapter V identifies which emission band systems for the ionospheric constituents (N_2, O_2, NO, O) are observable in the experiment. Finally, Chapter VI provides conclusions and suggestions for further research.

II. THE IONOSPHERE

The purpose of this chapter is to describe the region in space that is the focus of this experiment: the ionosphere. It is helpful to consider the entire atmosphere, before proceeding to focus on the ionosphere. The general atmospheric regimes are shown in Figure 2.01. Several of these regimes will be discussed in this paper. The first two regimes of concern are the homo- and heterospheres. The division of the atmosphere into these two sub-spheres is a result of significantly different processes that influence the layered structure of the ionosphere. Therefore, the homosphere and heterosphere will be discussed initially, followed by a description of the ionosphere, its sources, and its sublayers.

A. THE HOMOSPHERE AND HETEROSPHERE

The homosphere is the region of the atmosphere where turbulent mixing or eddy diffusion is the dominant dynamic mixing process. Atmospheric constituents N_2, O_2, Ar, He,and H, are uniformly distributed in this region. The homospheric air density falls off exponentially with increasing altitude as shown below:

$$\rho\ (z) = \rho_0\ e^{-(z/H)}. \qquad (2.1)$$

The altitude is given by z and H is the atmospheric density scale height. This is defined below as

$$H = \frac{k_B}{m}\frac{T}{g} + \frac{1}{T}\frac{dT}{dz} \qquad (2.2)$$

where k_B is the Boltzman constant, T is atmospheric temperature, g is acceleration due to gravity, and m is the mean molecular weight of the medium. This scale height is common to all constituents in the homosphere. The expression defining the scale height can be simplified by eliminating the second term when the temperature profile becomes isothermal and the temperature gradient goes to zero.

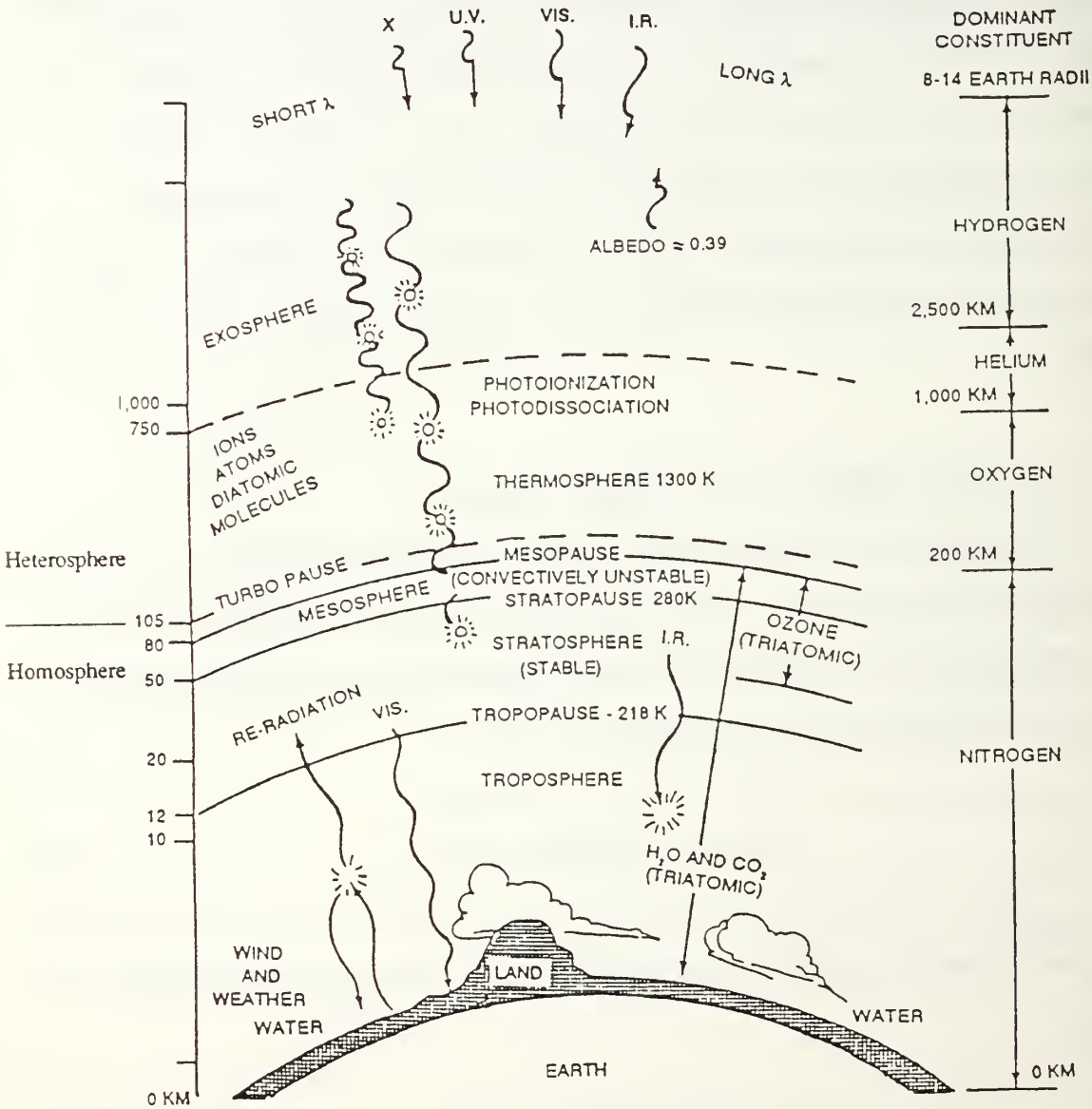

Figure 2.01 Atmospheric Regimes (Tascione, 1988)

The turbulent mixing processes associated with the air-earth interface diminish with increasing altitude. At around 100 km the dominant mixing mechanisms become molecular diffusion rather than eddy diffusion. As shown in Figure 2.01 the boundary is known as the turbopause. Atmospheric constituents begin to separate out based on molecular density, much as oil and water separate. The number density for each constituent falls off exponentially in proportion to its scale height. The density scale height is no longer based on mean molecular weight, but rather each individual molecular weight. This region is called the heterosphere.

B. THE IONOSPHERIC ENVIRONMENT

With increasing altitude, molecular diffusion rather than eddy diffusion becomes the dominant mixing process. This process combines with an increasing solar flux, and a decreasing atmospheric density to produce ions that have a sufficiently long lifetime to support the existence of a continuous plasma. This plasma is known as the ionosphere. The general relationship between incident solar flux and atmospheric gas concentration is shown in Figure 2.02. As is shown in this figure the lower limit of the ionosphere is typically 50 to 70 km (Tascione, 1988). The relatively wide range is primarily due to fluctuations in solar flux. The bold curve in Figure 2.02 represents the number density of ions over altitude The ionizing radiation is primarily the extreme ultra-violet and x-ray portion of the solar spectrum. The general shape of the ionospheric region indicates that ion density is negligible at very high altitudes. It then begins increasing in number density to a peak and decreases to a negligible intensity by an altitude of 50 km.

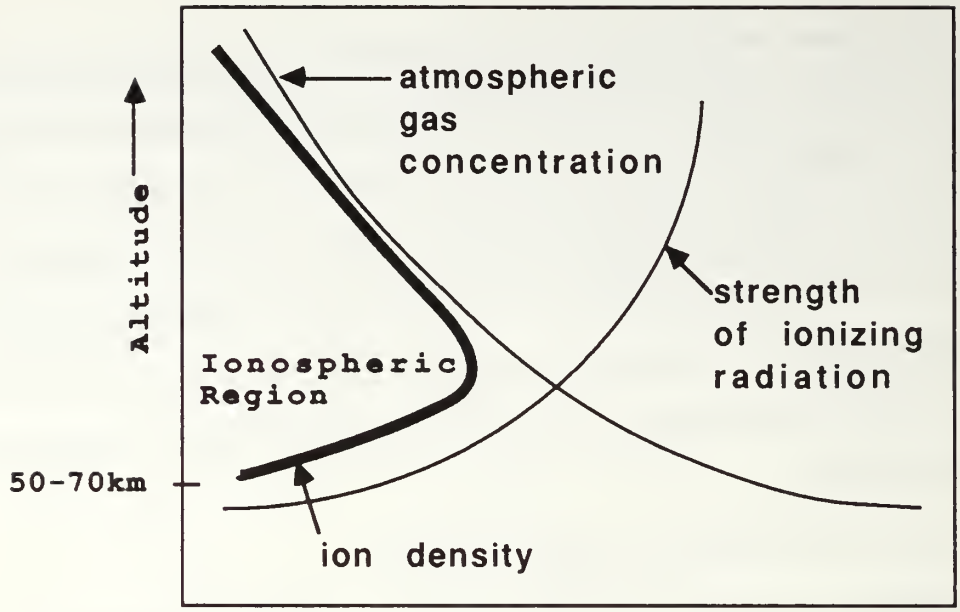

Figure 2.02 Generalized Ionosphere

The fluctuation in the upper and lower limits of the ionosphere, as well as fluctuations in the ion density vary in proportion to the level of solar activity. The vast majority of solar flux may be treated as a black body spectrum, based on the solar surface temperature, of about 5700 degrees kelvin. However, the high energy end of the spectrum, in the ultraviolet and x-ray regions, as well as the low energy end at radio frequencies exhibits significant fluctuations (Torr et al, 1979 for solar flux data over the solar cycle). The composition and vertical limits of the ionospheric layers are significantly influenced by this varying solar flux. The variable portion of the solar flux varies in predictable cycles. This solar cycle has a period of approximately eleven years. An accepted indication of solar activity is the measurement of a solar radio emission whose wavelength is 10.7cm. This measurement is designated the F10.7 and is taken at Ottawa, Canada. Both the F10.7 number and the sunspot number are shown in Figure 2.03. As the figure indicates, the F10.7 number tracks closely with the sunspot number.

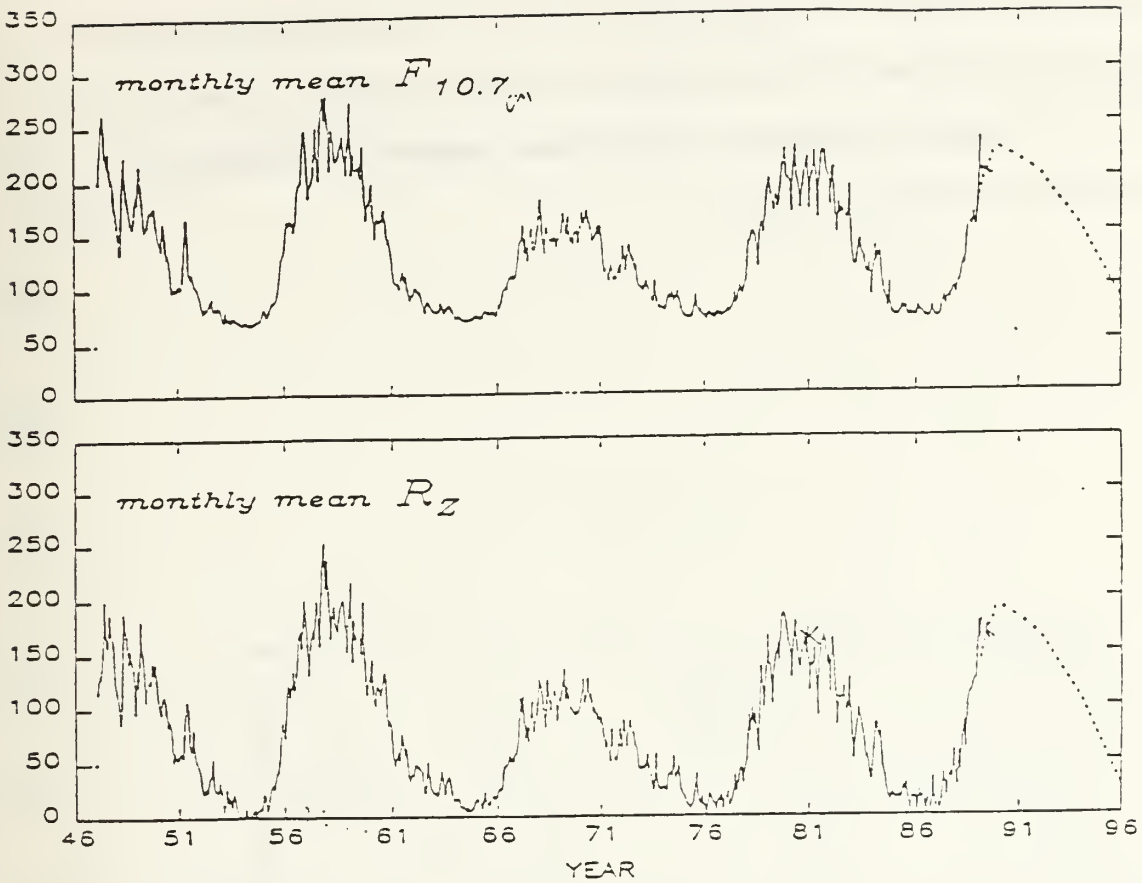

Figure 2.03 F10.7 and Sunspot Index(NRL, 1989)

The variable solar flux results in atmospheric temperature fluctuations, especially in the upper region of the atmosphere known as the thermosphere. The thermosphere is primarily heated by atomic oxygen absorption of extreme ultra-violet radiation (Tascione, 1988). Because, the extreme ultra-violet flux varies widely, the temperature of the thermosphere also varies. As is shown in Figure 2.04 this results in thermospheric maximum temperature ranges from 500 to almost 2000 degrees Kelvin. The predicted level of solar activity allows an atmospheric temperature profile to be estimated for a given location and date. An atmospheric temperature profile has been prepared for the MUSTANG experiment in Figure 2.05. The profile was obtained using the neutral atmospheric model MSIS-83 (Hedin, 1983). The model assumes a launch site latitude 33°

N, and longitude 105° W at White Sands, New Mexico. It also uses the predicted F10.7 value for an early February 1990 launch date of 215. The model also considers the launch time of day, which will be 1000 hours. The solar zenith angle is 72.47 degrees. Active solar conditions are used in the model.

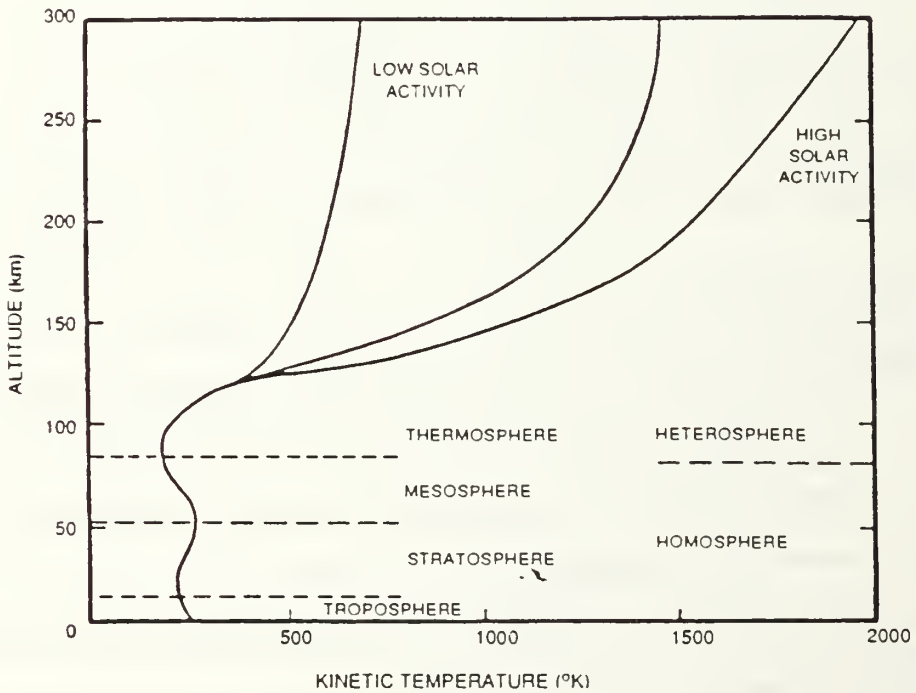

Figure 2.04 Atmospheric Temperature Ranges (Tascione 1988)

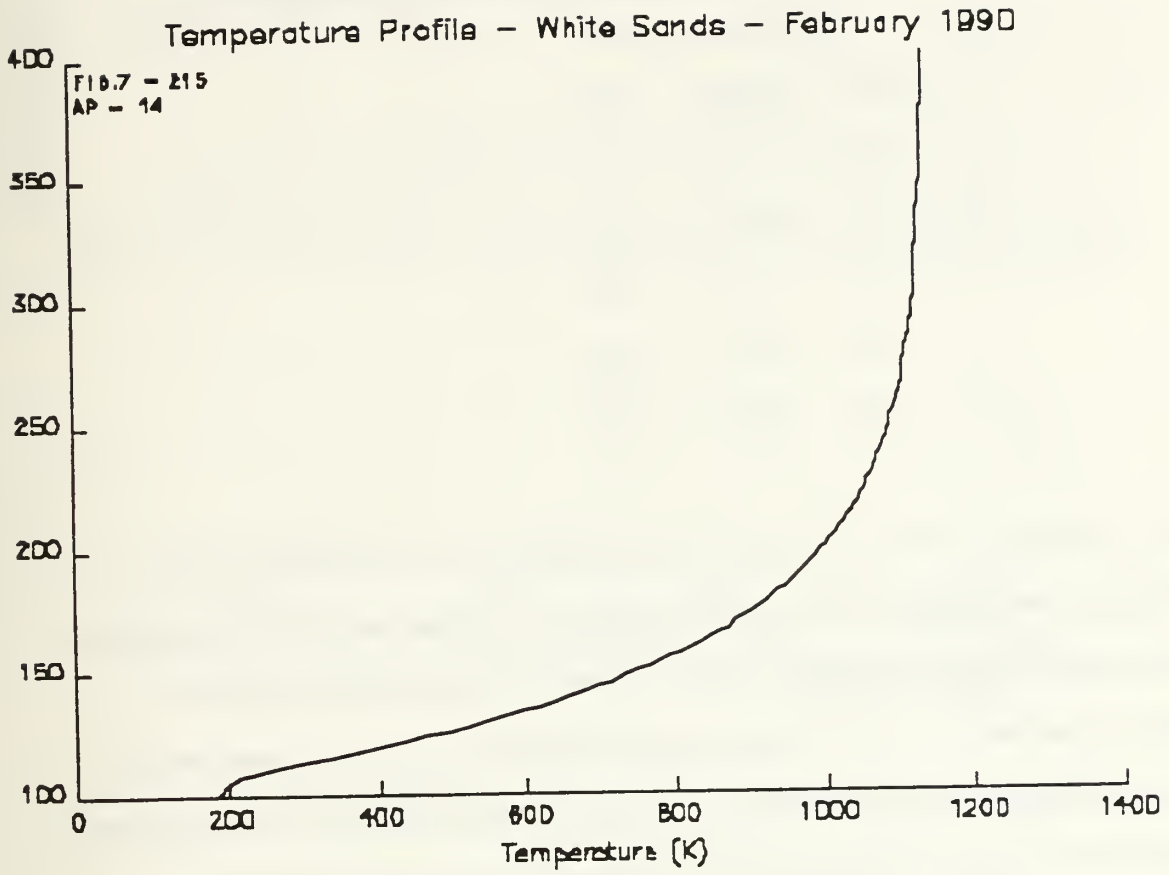

Figure 2.05 Projected Launch Date Temperature Profile (Hedin, 1983)

Solar radiation of sufficient energy to ionize atmospheric constituents is the primary ionizing mechanism throughout the ionosphere. The far and extreme ultraviolet, portion of the solar spectrum contain enough energy to ionize the principal constituents of the ionosphere. The minimum ionizing energy requirements for the constituents are determined by the ionizing work function of each species. These work functions are given in Table 2.1 for the primary atmospheric inhabitants

TABLE 2.01

IONIZING WORK FUNCTIONS FOR NEUTRAL PARTICLES

(Tascione, 1988)

Ion	KE(eV)	λ(Å)
N_2	15.58	795
N	14.50	851
O	13.20	908
O_2	12.07	1027
NO	9.26	1339

Table 2.02 indicates that the ionizing radiation requirement is at the highly variable, x-ray and extreme ultra-violet portion of the solar spectrum. The principal ionizing portion of the solar spectrum is shown in Figure 2.06. It is interesting to note that the strong Lyman Alpha solar emission at 1215Å will only meet the ionization energy requirement for the brelatively scarce NO molecule which results in its increased importance in especially the D region of the ionosphere. Photoionization is a direct energy absorption. The photoionization reaction is shown below for molecular oxygen:

$$O_2 + h\upsilon \Rightarrow O_2^+ + e$$

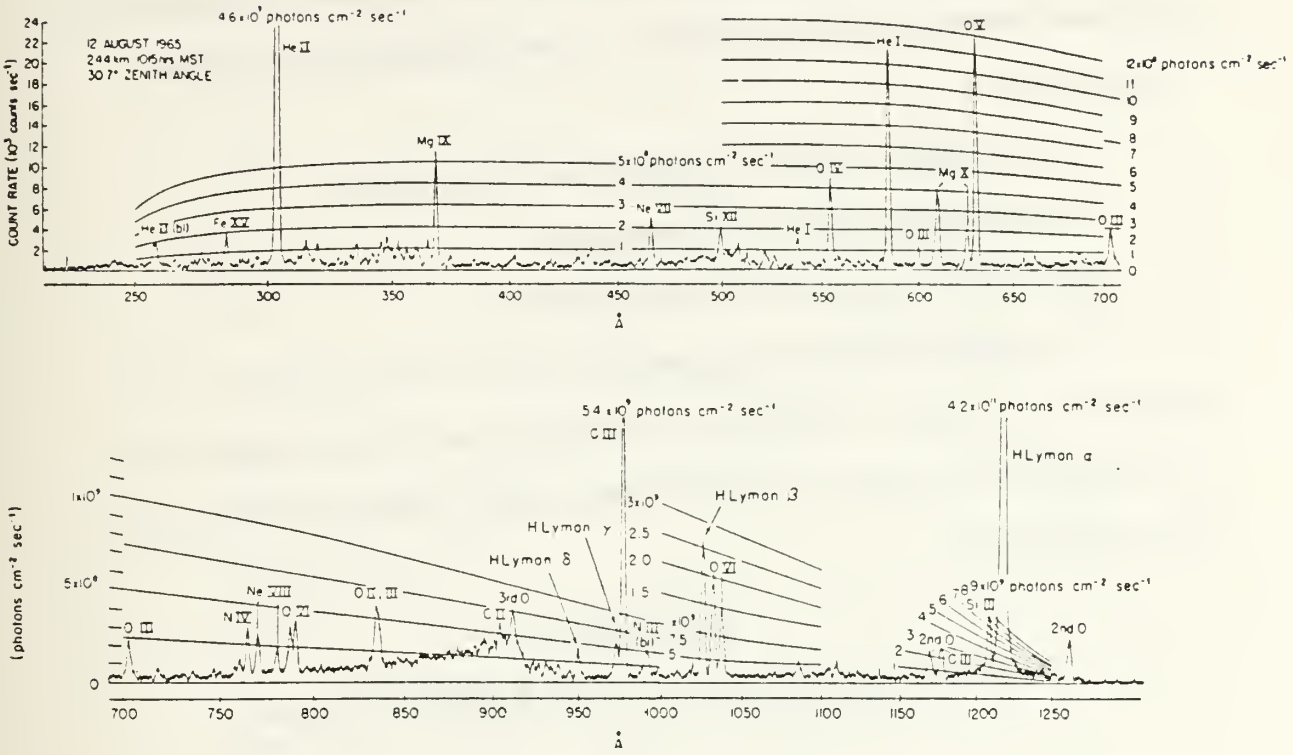

Figure 2.06 Solar Radiation 250-1250 Å (Banks & Kockarts, 1973)

This is the initial ionization process for each of the major atmospheric constituents. The kinetic energy of the electrons produced may be quite significant. These electrons are known as, photoelectrons. They will participate in one or even several additional collisions, before finally reaching thermal energies of around .025 electron volts (Banks and Kockarts, 1973).

C. THE IONOSPHERIC LAYERS

A closer examination of the ionospheric zone shown in Figure 2.02 reveals that it is not a smooth curve. The vertical structure of the ionosphere is changing constantly. It also

varies with time of day, solar activity, as well as with latitude. Despite fluctuating dramatically over time, and location, the ionosphere is always present. Furthermore, the ionospheric plasma has four distinct regions which are primarily the result of three competing factors:

- the atmospheric absorption of solar flux varies with altitude
- recombination of ions is density dependent
- atmospheric composition varies with altitude.

The ionospheric layers are designated the D, E, F1, and F2 region. The layer boundaries are not distinct. Although they are all present during the day, some do not survive throughout the night. Their general peak intensities correspond to the altitudes shown in Table 2.02.

TABLE 2.02

IONOSPHERIC REGIONS: PEAK HEIGHTS (km)

D - 90

E - 110

F1 - 200

F2 - 300

These layers, are called Chapman layers after Sidney Chapman, who first modeled them in 1931 (Chamberlain, 1987). The general shapes and locations of the Chapman layers are shown in Figure 2.07. The solid lines in the figure indicate electron concentrations under active solar conditions. The dashed lines indicate solar minimum conditions.

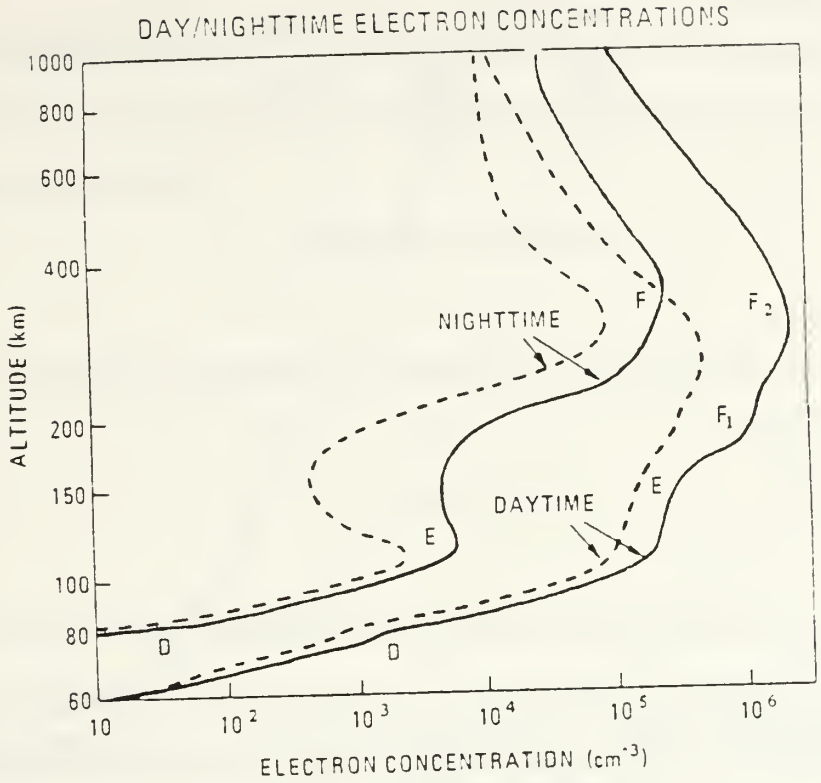

Figure 2.07 Chapman Layers (Chamberlain, 1987)

Before describing each ionospheric region it is necessary to describe the distribution of neutral species in the heterosphere, which overlays the E and both F layers of the ionosphere. The relative abundance of the neutral particles is distributed differently in each layer. The neutral atmospheric particle distribution is shown in Figure 2.08. Below about 175 km N_2 is the dominant species present. Above this altitude atomic Oxygen becomes the dominant species. O_2 and NO remain relatively minor constituents although as will be shown in Chapter V, both have significant roles to play in ionospheric photochemical processes.

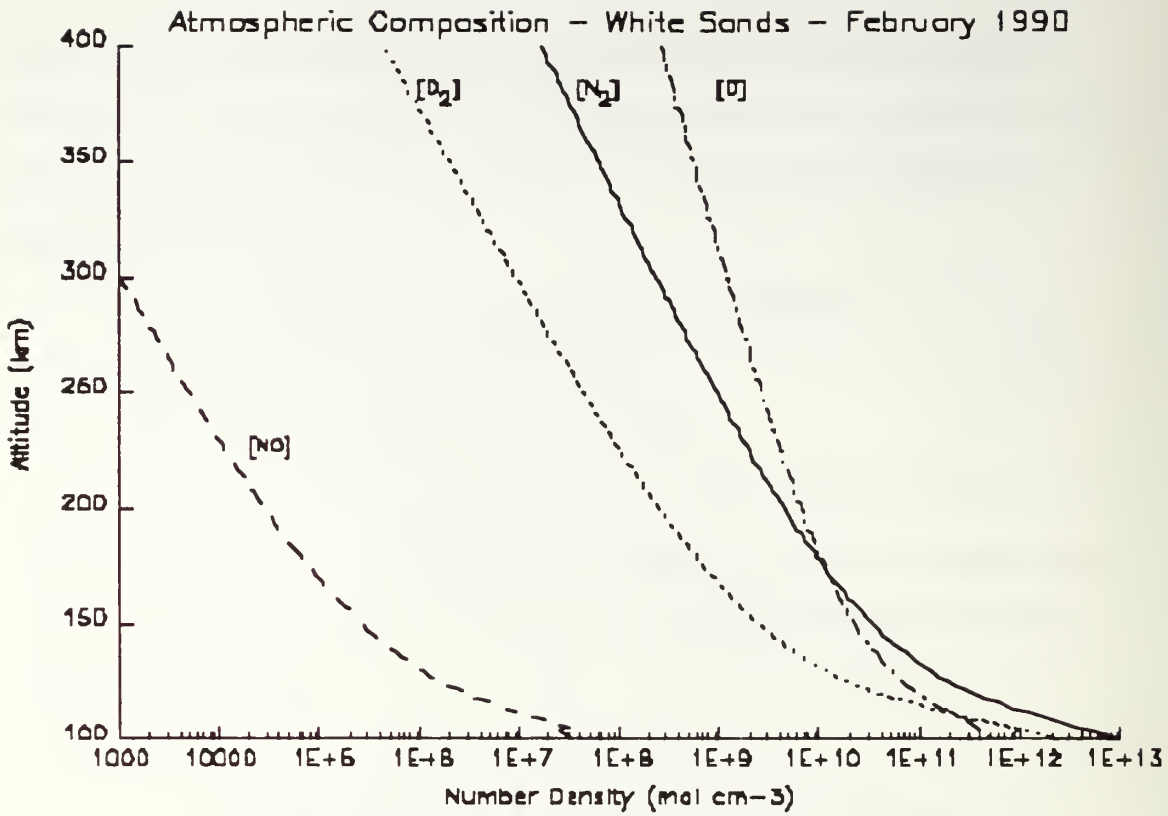

Figure 2.08 Primary Ionospheric Constituents

(Hedin, 1983 and Cleary, 1986)

The dominant processes that produce each ionospheric region is described below. A more detailed treatment of each region may be found in The Theory of Planetary Atmospheres, by Chamberlain (1987).

1. The D Region

The D region extends from 50 to about 90 km, with its peak near 90 km. The relatively high number density in this region results in a short mean free path between neutral particles, and electrons. The daytime electron density is about 1.4×10^4 electrons per cubic centimeter (el cm^{-3}). This produces a high recombination coefficient that causes the region to disappear at night. Solar Lyman-alpha radiation deposited in the region is the

principal ionization source for the NO molecule. Although photoionization is the dominant process, other interactions contribute to ion density. These include primarily three-body attachment as shown below:

$$O_2 + e + M \Rightarrow O_2^- + M.$$

A reaction of secondary significance is radiative attachment such as the example shown below:

$$O_2 + e \Rightarrow O_2^- + h\upsilon.$$

Principal loss mechanisms include photodetachment, which is the inverse of radiative attachment; collisional detachment, the inverse of three-body attachment; and mutual neutralization, such as $X^+ + Y^- \Rightarrow X + Y$. This last process indicates that the D region is characterized by a significant number of negative ions as well as electrons.

2. The E region

The E region extends from 90 to about 130 km. The nominal peak height is 110 km. The daytime density of 1.5×10^5 (el cm^{-3}) decays down to a night time density of 1×10^4 (el cm^{-3}) or less. The decreasing recombination coefficient allows its nighttime survival. Ionization primarily is the result of photoionization by solar extreme ultraviolet and soft x-rays. The ionization of atomic oxygen becomes significant. Negative ions are no longer significant contributors in the region. The principal ion loss mechanism is dissociative recombination such as:

$$NO^+ + e \Rightarrow N + O$$

3. F1 region

The F1 region extends from 140 to 200 km. Its daytime electron density is greater than the E region (2.5×10^5 el cm^{-3}vs. 1.5×10^5 el cm^{-3}) However, the principal

ions formed are O^+ and NO^+ which require an ionizing solar flux from the Lyman continuum as well as He emission lines. These sources disappear with sunset. Due to the relatively short ion lifetimes, the F1 layer disappears quickly at night. O^+ readily charge exchanges with O_2 and NO. These exchanges are given below:

$$O^+ + O_2 \Rightarrow O + O_2^+$$

$$O^+ + N_2 \Rightarrow NO^+ + N.$$

Once in these molecular forms the principal loss method is once again dissociative recombination.

4. F2 region

Beginning at 160 km, the F2 region extends all the way up and beyond 600 km, with a nominal peak density at about 300 km. Its day time density is around 10^6 (el cm^{-3}). The night time density drops by about one order of magnitude, to about 10^5 (el cm^{-3}). In the F2 region three significant factors adjust the ionization profile. First, the atmosphere becomes optically thin to most ionizing radiation; which adjusts the ion production equation. Second, ion-atom interchange becomes the dominant loss process instead of dissociative recombination. This results in the loss term diminishing as atmospheric density decreases. Ion production is from the same processes as the F1 layer. Atomic oxygen is the principal constituent and ion source in the region. However, since the loss term is diminishing with altitude the ion number density would increase indefinitely with height except for the effect of the third factor; ambipolar diffusion. The F2 region reaches the point where the chemical lifetime becomes longer than the diffusion lifetime. As a result positive ions diffuse downwards out of the region. This limits ion density towards the upper end of the region.

III. THE SOURCES OF THE ATMOSPHERIC AIRGLOW

A. BACKGROUND

The MUSTANG experimental objective to investigate ionospheric photochemistry is best accomplished by observing radiative emissions in the earth's airglow. Airglow emissions are omni-directional. An instrument's viewing angle is oriented to observe emission features without being overwhelmed by the solar flux. Specific emission features can be observed to identify the atomic or molecular transitions and therefore the molecular density of the species. Airglow emissions can then be converted to density profiles. These number densities can then be used to infer the electron and ion densities.

The sum of all radiative emissions from the extreme ultraviolet to the infrared comprises the atmospheric airglow. The airglow is optical radiation that arises from several types of interactions. Airglow emissions have three general sources:

- direct sunlight scattering
- electron impact excitation
- photochemistry of neutral constituents.

The primary source is direct sunlight scattering, or photoexcitation. Electron impact excitation is of secondary importance for allowed transitions, but it is the primary excitation mechanism for forbidden transitions. Some radiation is the result of a combination of these factors.

Solar ultraviolet radiation is primarily responsible for the airglow to be observed in the MUSTANG experiment. Figure 3.01 shows a typical nadir spectrum of the earth's airglow from 500 Å to 4000 Å. The primary EUV and FUV emission features are shown in this figure.The strong O_2 and O_3 absorptive bands shown in the figure result in the

suppressed airglow at wavelengths corresponding to these absorption bands. The figure also illustrates the emission bands to be observed by the Naval Research Laboratory instrument . The strong Lyman Alpha, and atomic Oxygen emission features are clearly visible between 500 and 1500Å. Conversely the NO and N_2 features in in the 2000 to 3000 Å range are not visible in a nadir view. This is an illustration of why the experiment must look across the limb to observe emissions in the 1800 to 3400 Å region.

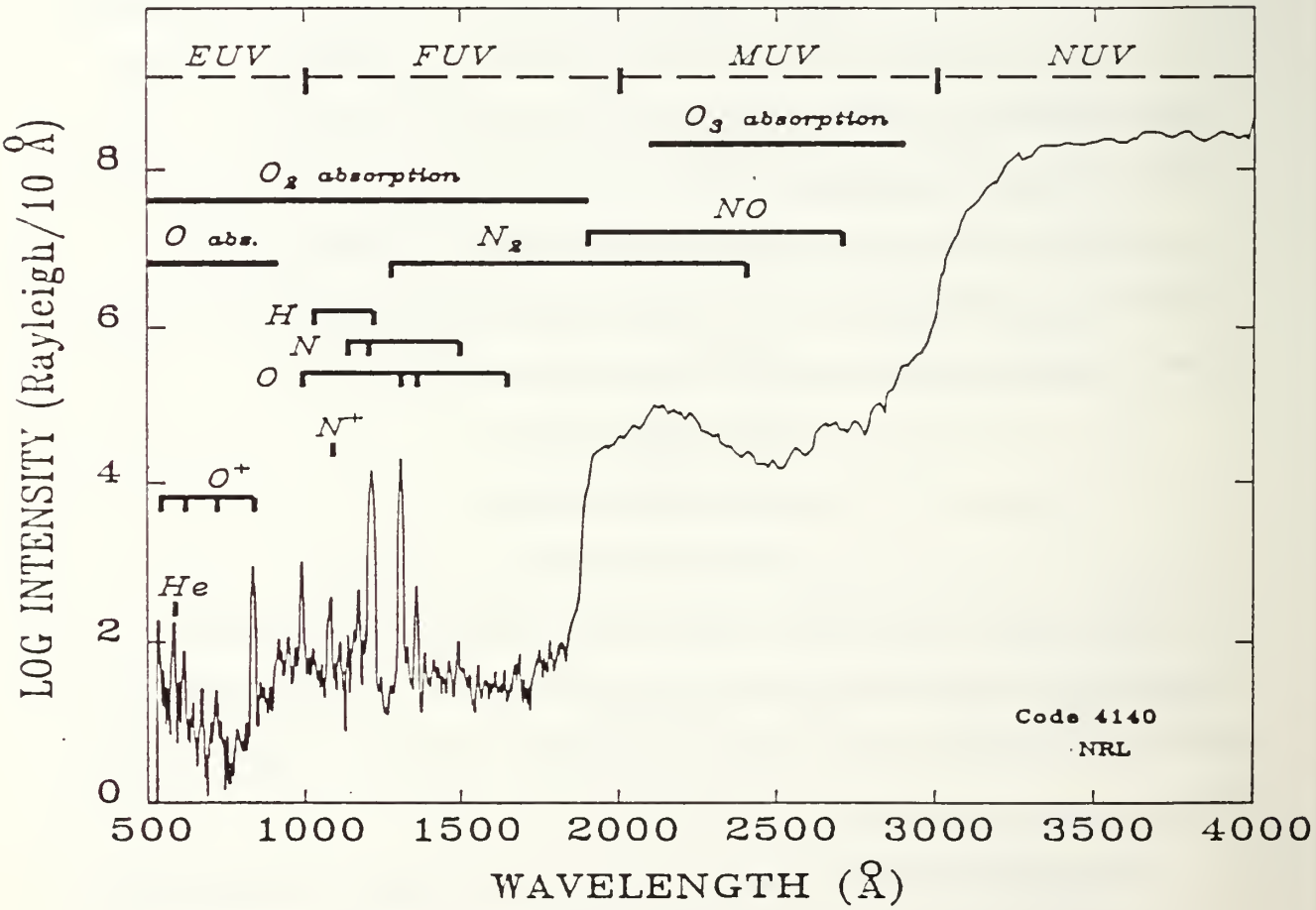

Figure 3.01 Earth Ultraviolet Airglow and Absorption/Emission Regions

The airglow is distinguished from another emission phenomenon, the aurora, by the energy source of the aurora. The energy sources for the aurora are solar electrons and protons, as opposed to solar flux as the primary source of the airglow. This results in the auroras confinement to polar regions and its sporadic occurrence. Conversely the airglow occurs continuously, over the entire sunlit portion of the atmosphere.

A. DIRECT SUNLIGHT SCATTERING

The primary process that results in the airglow is direct sunlight scattering, or photoexcitation. This process is similar to photoionization, the major ionization source. Photoexcitation occurs when the incoming photon energy matches the quantum energy levels required for a given atom or molecule. The photon will then be absorbed and leave the particle in an excited state. The normal lifetime of a particle in an excited state is very short; about 10^{-8} seconds (Eisberg, 1985).

The particle in the excited state can return to its desired ground state by emitting one or several photons. Photoexcitation that leads to the emission of photons is known as fluorescence. The entire process is known as fluorescent scattering. A special case of fluorescent scattering is resonant scattering. In the case of resonant scattering, the excitation and emission paths are the inverse of each other. A single photon, of the same wavelength as the excitation photon, is reradiated. The particle return path in general, may be along a direct or an indirect path. Multiple photons are emitted, for the general case where intermediate states lie between the excited state and ground. Only electronic excitation levels are available to atoms. Molecular excitation may result in electronic, vibrational, or rotational transitions, or combinations of these three. Energy requirements vary for each type of transition. Electronic transitions require between one and ten electron

volts, while vibrational transitions require between one tenth and one electron volt, and rotational transitions are a factor of ten less than vibrational transitions.

Transitions are considered allowed or forbidden depending on their compliance with quantum selection rules. The actual selection rules that apply to molecular transitions will be discussed further in Chapter IV. A transition that meets all selection rule requirements is an allowed transition. A transition that violates a selection rule at one level may be forbidden; but may or may not be strictly forbidden. For example a transition forbidden as electric dipole radiation may be allowed with a lower probability as a magnetic dipole, or electric quadrupole transition.

An excited state whose only path to the ground state is through a forbidden transition is called a metastable state. Usually, the particle can still reach the lower state, but the probability of doing so becomes much smaller than if the lower state was an allowed state. Lifetimes in the excited state can become relatively long. They can be on the order of seconds as is the case for one of the emission bands to be examined in Chapter V. Metastable states are much more likely to transfer energy as a result of a collision with another particle prior to emission. This process is called quenching.

It is also of note that molecules in an excited state may dissociate, or predissociate, rather than emitting a photon. An absorption leading to an excited state above dissociation or predissociation energy, will dissociate rather than emit a photon. These processes are best shown graphically. Figure 3.02 shows two simplified potential energy diagrams for the O_2 and NO molecules. As shown in the figure, an O_2 molecule excited to the $A^3\Sigma^+_u$ state at a vibrational level above the dissociation threshold energy will dissociate to the $O(^3P) + O(^3P)$ atoms. This may be viewed as a path to climb out of the electronic potential well. Conversely, a molecule of NO excited to a vibrational level above the predissociation energy of the $C^2\Pi$ state may predissociate along the $a^4\Pi$ path to become

$N(^4S^0) + O(^3P)$ atoms. This may be viewed as a hole in the potential energy well. The result of both of these processes is that absorptions will not result in emissions.

O_2 Potential Energy Diagram

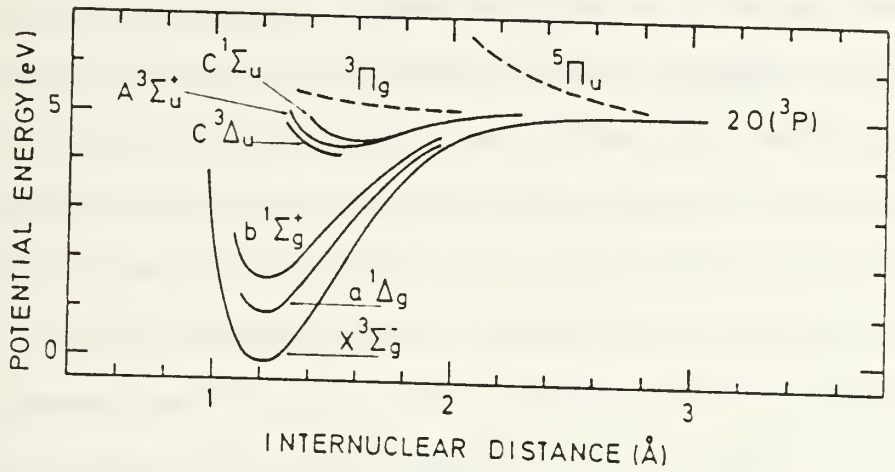

NO Potential Energy Diagram

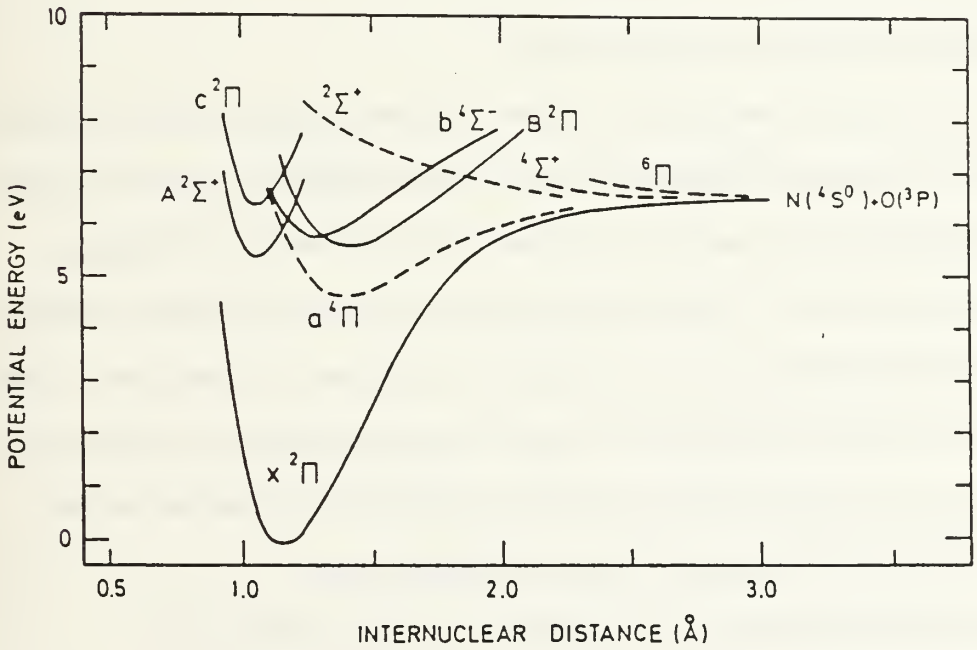

Figure 3.02 Dissociation and Predissociation Paths (Chamberlain, 1987)

B. ELECTRON IMPACT EXCITATION

The primary excitation source for atoms or molecules is solar radiation. However, photoexcitation is forbidden for some of the constituents in the upper atmosphere. In this case, electron impact can cause the excitation of the particle to an excited state where it can than emit a photon upon undergoing a forbidden transition. Electron impact scattering is an inelastic collisional process. The probability of an emission resulting from an electron collision with a neutral particle depends on several factors. Electron impact excitation is dependent on the molecular number density, electron impact cross-section, and the electron flux. Since the electron flux is not monoenergetic, and since the molecular electron absorption cross-section is dependent on electron energy, an actual calculation requires an integration over available energies. This will be done for several forbidden emissions in Chapter V.

C. PHOTOCHEMICAL REACTIONS

A third relatively minor source of airglow emissions is radiation resulting from the photochemistry of neutral constituents. Photochemical processes are initiated in the same manner as photoabsorptive processes. A photon is absorbed leaving the absorbing molecule in an excited state. This excited state could be an excited rotational or vibrational level or an excited electronic state. It could also be a dissociated or ionized state. In this excited state the molecule may enter into secondary chemical reactions that would not be available from the ground state. Upon completion of the chemical interaction the new species emits a photon. This process is called chemiluminescence.

Photochemical processes are complicated because they are non-local thermodynamic equilibrium processes. Each rate of reaction must be calculated separately.

Addressing each photochemical process is beyond the scope of this thesis. Chemiluminescence is an insignificant contributor to the day airglow. It becomes important at night when other excitation sources are not present.

IV MOLECULAR SECTROSCOPY

Chapter IV addresses molecular transitions, and synthetic spectra . These are two broad regions that comprise molecular spectroscopy. The vast majority of emission processes to be observed in the MUSTANG experiment are a result of molecular transitions. Furthermore, this chapter is exclusively concerned with diatomic molecules. Diatomic molecules are the dominant type found in the atmosphere. Molecules other than diatomic introduce coupling schemes beyond the scope of this thesis. More specifically, emissions will primarily occur as a result of vibrational transitions between molecular electronic states. This type of emission process is one of several possible types of diatomic molecular transitions. Molecular transitions occur between rotational and vibrational levels as well as between electronic molecular states. It may also be between some combination of these three. Each type of transition is characterized by quantum energy jumps rather than a continuous emission spectrum. All three types of molecular transitions will be addressed, with emphasis on vibrational transitions between electronic states. Additionally the compilation of synthetic spectra will be addressed. A more detailed account of molecular transitions is provided by Herzberg, in his definitive volume, Spectra of Diatomic Molecules (Herzberg, 1950).

A. MOLECULAR TRANSITIONS

This section is concerned with rotational and vibrational levels, as well as electronic states. It is also concerned with transitions between these states. These transitions range in energy from the least energetic rotational transition, to the most energetic electronic transition. They are in effect a nested sequence of transitions. A pure rotational transition

can occur between two rotational levels in the same vibrational level and electronic state. However, as vibrational and electronic transitions come into the picture, subordinate level transitions must be taken into account.

1. Rotational Levels and Transitions

A diatomic molecule as shown in Figure 4.01, can be represented as a dumbbell. The two masses m_1 and m_2 are connected by a rigid rod of length r with the center of mass at s. The two masses represent the atomic nuclei, where the vast bulk of the atomic mass is concentrated. As opposed to an atom, the molecule can undergo two forms of motion. It can rotate around the center of mass axis and the two nuclei can vibrate relative to one another along the internuclear axis. The two masses are not in fact rigidly bound. This perturbation to the rigid rotator and vibrator will be addressed later in this chapter. At this point it is adequate to note that the internuclear axis will vary with the speed of rotation, or strength of oscillation.

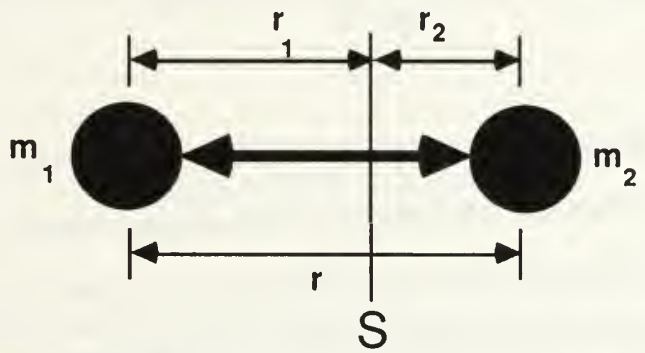

Dumbbell Model of a Diatomic Molecule

Figure 4.01 Dumbbell Model (Herzberg, 1950)

The simplest form of motion the two components can undergo is rotation around the center of mass axis S. Quantum theory requires the velocity of this rotation to

take on discrete values. Isolating the molecular motion to pure rotation results in the system's angular momentum as

$$P = I\omega . \qquad (4.1)$$

The classical kinetic energy of rotation would be $E = \frac{1}{2} I \omega^2$. The classical energy becomes the expression

$$E = \frac{P^2}{2I}. \qquad (4.2)$$

P is from equation 4.1, and the moment of inertia I, is dependent on the reduced mass. The solution to the Schrodinger equation yields available energies of the form shown

$$E = \frac{h^2 J(J + 1)}{8\pi^2 I} . \quad (4.3)$$

In Equation 4.3, h is Planck's constant, I remains the moment of inertia, and the rotational quantum number J is introduced. J is limited to positive integer values. The energy of the system E, will increase quadratically with increasing J as is indicated in Equation 4.3. The angular momemtum of the system in some quantum state J becomes

$$P = \frac{h}{2\pi} \sqrt{J(J + 1)} \approx \frac{h}{2\pi} J . \quad (4.4)$$

Classical electrodynamics requires a changing dipole moment to produce an emission. Any diatomic molecule composed of two heteronuclear atoms will possess a permanent dipole.

Diatomic molecules with a permanent dipole moment will produce an emission when rotated. The quantum mechanical system indicates that the system will have a series of discrete energy levels whose energy increases quadratically as J increases. A transition between two of these available energy states will result in a discrete rotational emission feature. The wave number ν, is introduced at this time. Wave number is equal to the reciprocal of the wavelength ($1/\lambda$) or frequency divided by the speed of light. Wave number carries units of cm^{-1} (number of waves per centimeter). The wave number for the rigid rotator is given by

$$\nu = \frac{E'}{hc} - \frac{E''}{hc} \quad . \quad (4.5)$$

The upper and lower energy states are indicated by E' and E", respectively, while h is Plancks constant and c is the speed of light. The rotational term F(J), is also introduced, and depends on the physical characteristics of the molecule and dependent on J. The relationship is

$$F(J) = \frac{\Delta E}{hc} = BJ(J + 1) \quad . \quad (4.6)$$

The constant B is known as the rotational constant of each molecule and is given by $B = \frac{h}{8\pi^2 cI}$.

Only certain rotational transitions are allowed for a given excited state J'. The available states are governed by what are known as selection rules. Selection rules for the rotational quantum number J, are $\Delta J = \pm 1$. This requires that J vary by one higher or one lower quantum level in either absorption or emission for a rotational transition.

2. Vibrational Levels and transitions

A perturbed, diatomic molecule can also undergo vibratory motion. The configuration for the molecule shown in Figure 4.01 is still appropriate, however a second mode of motion is now considered. A classical picture would consider the two molecules as connected by a spring. Perturbing the system would result in simple harmonic motion. The equation of motion is a straight forward result of Hooke's Law: F = -kx, where k is the force constant . The vibrational frequency of the molecule is defined as $\nu_{osc} \equiv \frac{1}{2\pi}\sqrt{\frac{k}{\mu}}$ where μ is the reduced mass. For a given vibrational state, the vibrational energy level, and the resultant vibrational term G(v) is given by

$$G(v) = \frac{E(v)}{hc} = \omega(\upsilon + \tfrac{1}{2}). \qquad (4.7)$$

The factor ω, equal to ν_{osc}/c, is introduced in equation 4.7, and is a constant for each molecule. The vibrational quantum number v is also introduced. The vibrational quantum number is restricted to positive integers. It is of note that when v is equal to zero; the lowest vibrational state, the vibrational energy equals $\frac{1}{2}\omega$, rather than zero. Additionally the linear dependence on v, results in equidistant energy levels, for increasing vibrational levels.

Vibrational selection rules, restrict available transitions between higher and lower states to unity; $\Delta v = \pm 1$. Homonuclear molecules such as N_2, have a zero dipole moment. Vibrational transitions can only occur as quadrupole transitions for these molecules. Quadrupole radiation has a very small probability with respect to dipole radiation, and is negligible under normal circumstances. The selection rule $\Delta v = \pm 1$ is not rigidly adhered to for asymmetric molecules such as NO. Dipole allowed transitions

have a weak probability of emission when $\Delta v > \pm 1$. This is as opposed to the rotational case where the selection rule is rigidly adhered to.

The molecule can undergo simultaneous vibrational, and rotational motion. The total energy in the rotating oscillator case is approximately $T = G(v) + F(J)$. The period of oscillation is on the order of 10^{-14} seconds, while the period of rotation is about 10^{-12} seconds. This means that the rotational position changes slowly compared to the oscillating motion. For a given vibrational energy level, there are a series of rotational levels available. The selection rule remains $\Delta J = \pm 1$ for a specific vibrational level. The series of vibration-rotation transitions is called a band. The $\Delta J = 1$ case forms one branch, known as the R-branch and the $\Delta J = -1$ case forms the P-branch. An illustrative example of a vibrational-rotational band system, with P and R branches is shown in Figure 4.02.

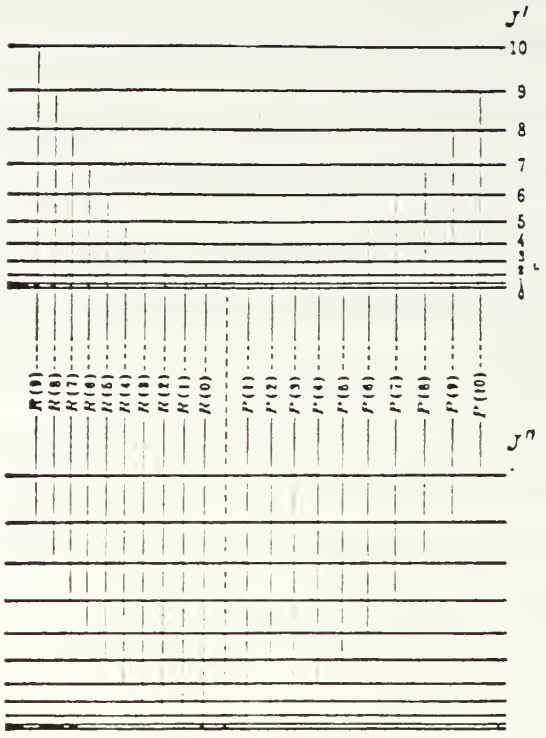

Figure 4.02 Vibrational-Rotational Energy Level Diagram

(Herzberg, 1950)

3. Electronic States, Nomenclature, and Transitions

a. Electronic States

The nuclei of a molecule repel each other. The molecule is held together by what is in effect an entire molecular group of electrons. The electron cloud interaction with the nuclei results in a strong axial electric field. The orbital configuration of this electron cloud determines the electronic energy of the system. The electrons are moving much faster than the nuclei, so the electronic energy corresponds to each temporary position of the nuclei. Work must be done against the Coulomb repulsion of the nuclei, and work is required to change the electronic energy, in order for the position of the nuclear elements to change. There must be some minimum value in order for the electronic state to be stable. The shape of the potential energy curves for electronic states indicates whether

the state is stable or unstable. Without a minimum in the potential energy curve, the two atoms will repel each other at any internuclear distance. This is an unstable state. Figure 4.03 illustrates several potential curves for different electron states for a Li_2 molecule. As is shown in the figure, the $^1\Pi_u$,$^1\Sigma^+_u$ and $^1\Sigma^+_g$ states all possess minimum points, and are stable states. The $^3\Sigma^+_u$ state has no minimum and is an unstable state.

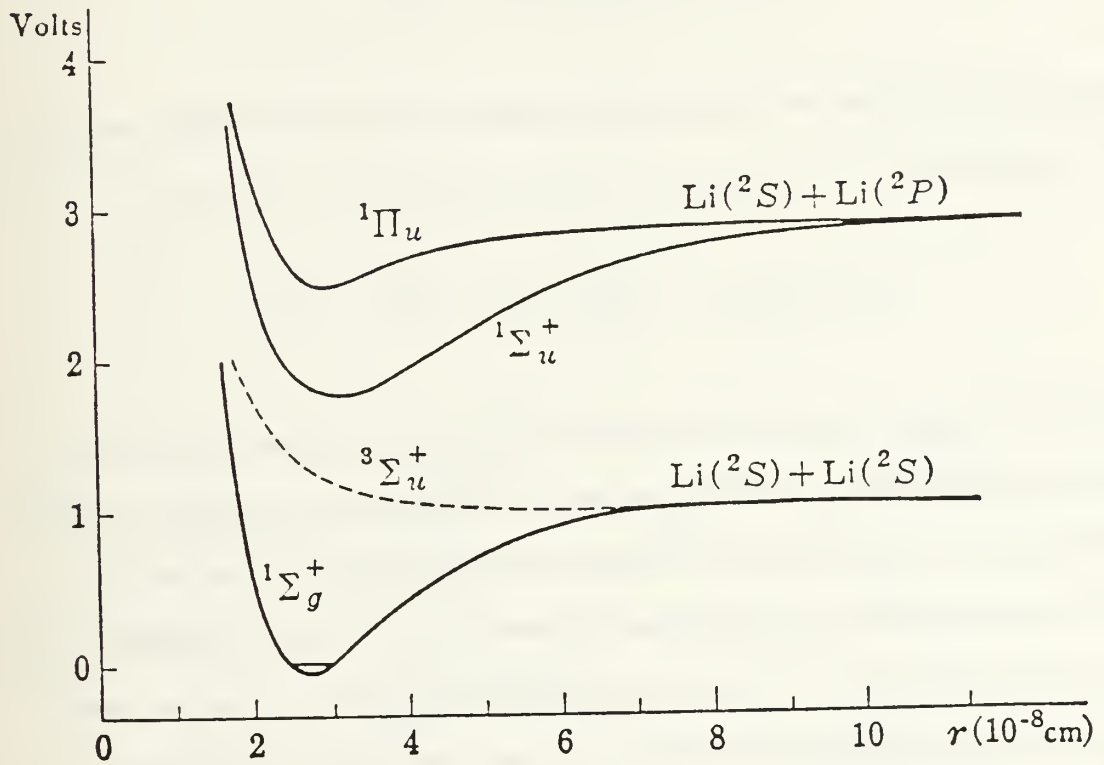

Figure 4.03 Stable and Unstable Potential Energy Curves

(Herzberg, 1950)

b. Electronic Transitions

In a similar manner in which purely rotational transitions were extended to include vibrational-rotational transitions, vibrational-rotational transitions can now be extended to include transitions between electronic states. The total energy of the molecule in a given energy state is defined as the sum of the rotational, vibrational and electronic components. This definition is given by

$$E = E_e + E_v + E_r . \qquad (4.8)$$

The change in energy from one specific state to another is the sum of the energy changes of each component as

$$\Delta E = \Delta E_e + (E_v' - E_v'') + (E_r' - E_r''). \qquad (4.9)$$

For any given change in electronic state, there is a wide range of possible vibrational and rotational transitions. Thus, the transitions become a band rather than a single line. Figure 4.04 illustrates the concept of nested rotational, vibrational and electronic levels. This figure illustrates the nesting concept between electronic states. For a given transition between two electronic states, there are numerous vibrational transitions possible. Each vibrational transition is in fact a band of all possible rotational lines for each particular upper and lower vibrational level. The sum of these bands form the band system representing emission or absorption features between two electronic states.

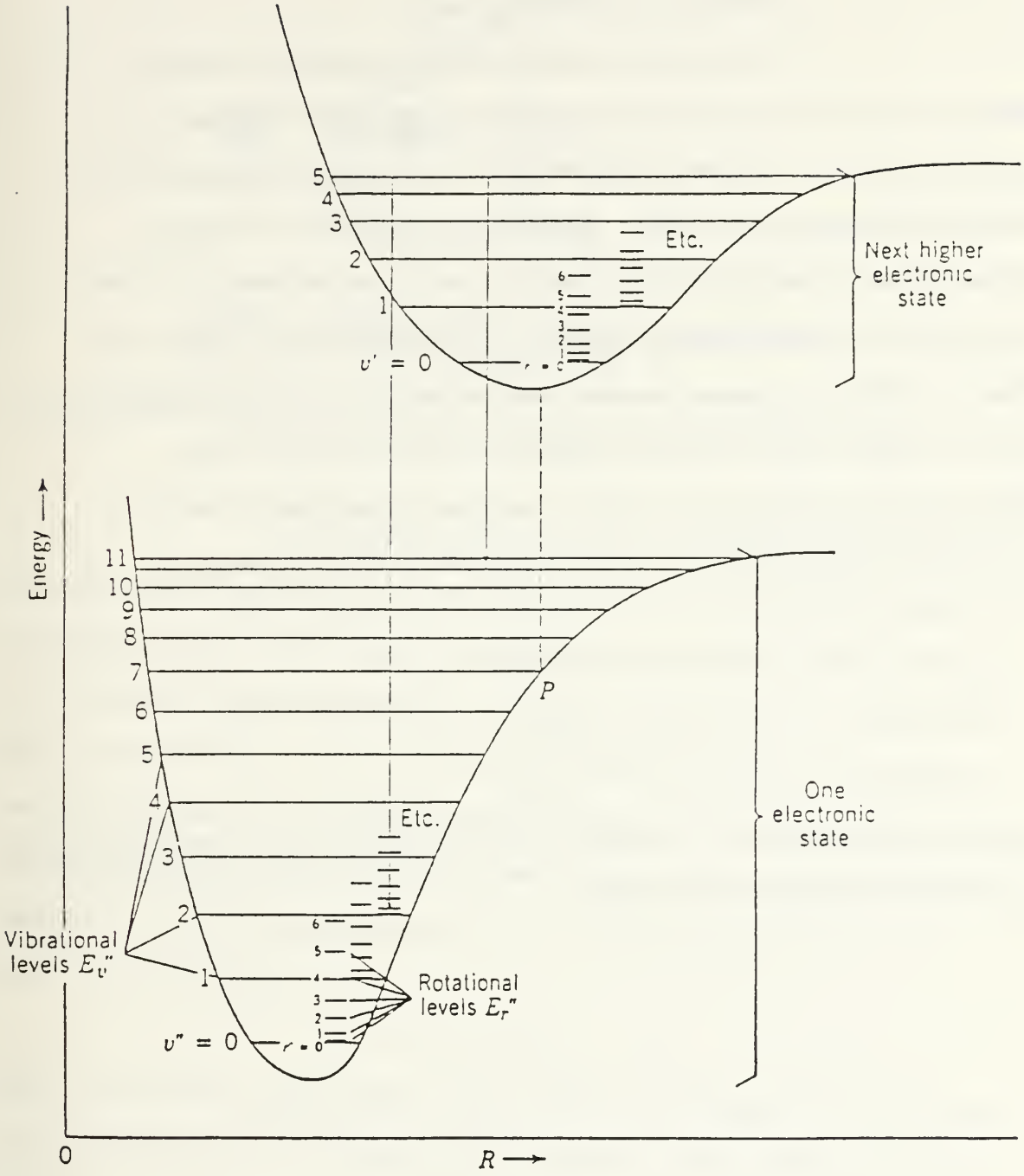

Figure 4.04 Rotational, Vibrational, and Electronic Levels

(Eisberg, 1985)

c. Electronic State Nomenclature

The internal molecular electric field is symmetric about the internuclear axis. The molecular electron's motion in this field results in a total orbital angular momentum, L. As shown in Figure 4.05, L is not a constant of the motion as it precesses around the axis of symmetry. However, the component of L along the internuclear axis is a constant of the nutation. This component designated Λ, is a better indication of the molecular electronic state than L. The electronic configurations, and indeed the labeling of successive electronic states, is analogous to the atomic case. The symbol $\Lambda = |M_L| = 0,1,2,...$ L is used to designate a particular electronic state. Furthermore, each electronic state is given a Greek letter to distinguish the molecular electronic state from its atomic equivalent. The lower four molecular states are:

$0 - \Sigma$

$1 - \Pi$

$2 - \Delta$

$3 - \Phi$.

It should be noted that for $M_L > 0$, electronic states will exhibit double degeneracy since for a given Λ, M_L can be positive, or negative.

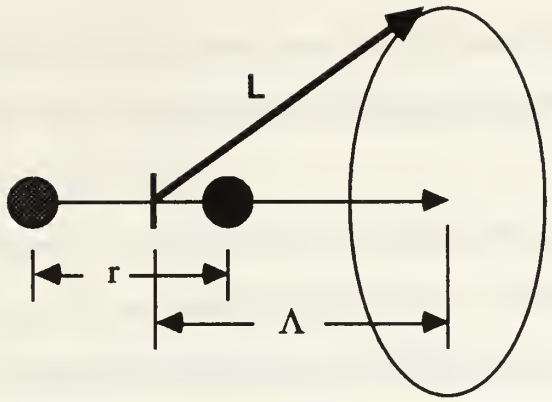

Orbital Angular Momentum Precession about the internuclear axis r

Figure 4.05 Precession about the Internuclear axis (Herzberg, 1950)

Electron spin in molecules results in a multiplet structure for either a particular band or an individual line. Just as in the atomic case, an odd or even number of total electrons results in a half integer or integer total spin, respectively. The resultant spin S is unaffected by the electrostatic field. It will precess in the presence of a magnetic field. When Λ is greater than zero, the orbital motion of the electrons results in the generation of an internal magnetic field in the direction of the internuclear axis. The spin interaction, S, with this magnetic field will precess in much the same manner as L. Also in much the same manner as L, a constant component M_S will exist for a given spin precession. M_S has specific values designated Σ, where

$$\Sigma = S, S-1, S-2, \ldots -S.$$

This is a total of 2S+1 possible values. This also indicates the multiplicity of the state. In a manner similar to atomic classification, the spin is written as a left superscript. Where $\Lambda \neq 0$, the sum $\Lambda + \Sigma$ is written as a right subscript.

Some additional points of classification for electronic states are noted at this time. The ground state of a diatomic molecule is labeled with X, while

successive excited states, of the same multiplicity, are labeled A, B, C, and so on. Similarly, successive excited states where multiplicity differs by two are designated by a, b, c, . . .

The nomenclature being discussed above, is repeatedly used in the potential energy diagrams in Chapter V where various emission band systems are investigated. Emission band systems are generally named for their discoverer. For example the N_2 Vegard-Kaplan bands were discovered by Vegard and Kaplan (JPCRD, 1977). These bands are designated as $A^3\Sigma_u^+ - X^1\Sigma_g^+$. This indicates a transition from the first excited electronic state A, to the ground state X for the case where both upper and lower states are in the Σ electronic configuration. Since $\Lambda = 0$ for the Σ state, the right subscript of $\Lambda + \Sigma$ provides no additional information. In this case the right subscript becomes u and g which indicates an odd to even electronic state.The spin goes from Σ equal to three to Σ equal to one. This violates one of the selection rules that govern electronic transitions. These selection rules are discussed in the next section.

d. Selection Rules

Selection rules governing electronic transitions are not as simple as those for rotational or vibrational levels. The selection rules that govern allowed transitions are shown in Table 4.01. Allowed transitions will comply with these selection rules. This will result in electric dipole radiation. The ΔJ selection rule gives rise to three branches although more branches may result from a particular transition. Depending on the multiplicity of the upper and lower states the three branches are designated R, P and Q. The $+ \Leftrightarrow -$ selection rule in Table 4.01 refers to positive and negative terms. Only positive to negative transitions and vice versa are allowed. The $s \Leftrightarrow s$ and $a \Leftrightarrow a$ selection rules refer to symmetric and antisymmetric terms. Only symmetric to symmetric or antisymmetric to antisymmetric transitions are allowed. The $g \Leftrightarrow u$ selection rule requires

only even states to odd and vice versa are allowed. These selection rules are subject to the limitations arising from compliance with coupling schemes to be covered in the next section (Hund's case (a) and (b)).

TABLE 4.01

APPROXIMATE MOLECULAR SELECTION RULES

(Herzberg, 1950)

$\Delta S = 0$

$+ \Leftrightarrow -$

$s \Leftrightarrow s$

$a \Leftrightarrow a$

$g \Leftrightarrow u$

$\Delta\Lambda = 0, \pm 1$

$\Delta J = 0, \pm 1$

There are exceptions to these selection rules. One exception of significance is that Σ^+ to Σ^- is not allowed but Σ^+ to Σ^+, and Σ^- to Σ^- is allowed. Other exceptions will be dealt with on an individual basis in Chapter V.

Violation of one of the selection rules in Table 4.01 does not mean the transition is rigidly forbidden. The transition may be allowed as magnetic dipole or electric quadrupole radiation which introduces additional selection rules. These rules are supplemental exceptions to the selection rules of Table 4.01. The Herzberg bands for molecular oxygen as well as the Vegard-Kaplan and Lyman-Birge-Hopfield bands for molecular nitrogen all violate at least one of the selection rules listed in Table 4.01 (see

Chapter V). Table 4.02 lists selection rules that apply for magnetic dipole and electric quadrupole radiation.

TABLE 4.02

SUPPLEMENTAL SELECTION RULES FOR ELECTRIC QUADRUPOLE AND MAGNETIC DIPOLE RADIATION

(Herzberg, 1950)

$+ \Leftrightarrow +$

$- \Leftrightarrow -$

$g \Leftrightarrow g$

$u \Leftrightarrow u$

B. SYNTHETIC SPECTRA

1. Overview

The previous section defined molecular transitions along with the nomenclature and selection rules that apply to molecular transitions. In this section the wavelengths and relative intensities of these transitions will be identified. The synthetic spectra that are produced by these techniques can then be used to link observed emissions with the emitting molecule. Unique emission features allow observers to identify the "fingerprints" of each emitting species. The techniques described in this section can be used by computer modelers to develop synthetic spectra for each emission band that will be observed.

2. Line Positions

The magnitude of the energy difference shown in equation 4.9, divided by hc, for either an emission or absorption, is known as the line position. Line position

carries units of cm^{-1}. Another descriptive name is the wave number. The line position σ, follows from the change in the appropriate parameters for the electronic, vibrational, and rotational contributions to the total. These are: the total electronic energy T_e, the vibrational energy F(J), and the rotational energy G(V). The vibrational and rotational energies remain as were discussed earlier in Chapter IV. For a given transition from an upper state (T_e',v',J') to a lower state (T_e'',v'',J'') , the line position σ is expressed as is

$$\sigma = T' - T'' + G'(v) - G''(v) - F'(J) - F''(J). \qquad (4.10)$$

The electronic portion of the entire band system $\sigma_e = T' - T''$ remains constant. This can be used to simplify Equation 4.10. The line position for a particular band system can be written as

$$\sigma = \sigma_e + G'(v') - G''(v'') - F'(J') - F''(J''). \qquad (4.11)$$

For any v' to v'' transition, there may be hundreds of rotational transitions. The wave number for any one of these lines becomes as is shown by:.

$$\sigma_{j'j''} = \sigma_0 + F'(J') - F''(J''). \qquad (4.12)$$

The σ_0 term is known as the band origin or band head. Its value is given by

$$\sigma_o = \sigma_e + G'(v') + G''(v''). \qquad (4.13)$$

At this point the rigid rotator and simple harmonic oscillator approximations need to be addressed. The constants used to determine line position are given by Huber and Herzberg (1979). However, these constants include anharmonicity and non-rigid rotator effects. In this case the vibrational term becomes

$$G(v) = \omega_e(v + \frac{1}{2}) - \omega_e x_e(v + \frac{1}{2}). \qquad (4.14)$$

The values for ω_e and x_e are constants of each molecule and the second term accounts for anharmonicity. The rotational term becomes

$$F(J) = B_v J (J + 1) - D_v J^2(J + 1). \qquad (4.15)$$

where the second term accounts for the non-rigid rotator. The factors B_v and D_v depend on the vibrational level. The expression defining B_v is given by

$$B_v = B_e - \alpha_e(v + \frac{1}{2}) + \text{higher order terms.} \qquad (4.16)$$

Similarly the expression for D_v is

$$D_v = D_e - \beta_e(v + \frac{1}{2}) + \text{higher order terms.} \qquad (4.17)$$

The constants B_e, α, D_e, and β are all found in Huber and Herzberg.

The spin $\Sigma \neq 0$ and orbital angular momentum $\Lambda \neq 0$ contribute to molecular degeneracy through several coupling schemes. The rotational term values in these cases are highly dependent on the coupling between Λ and Σ. In 1927, Hund (1927) first considered five possible cases of coupling between Λ and Σ. The first two of these are

applicable to molecules with emission bands between 1800 and 3400 Å and will be examined further. The total electronic angular momentum vector Ω is the algebraic sum of the Λ and Σ components. The algebraic rather than vector sum shown in equation 4.18 is appropriate since both terms are aligned along the internuclear axis.

$$\Omega = | \Sigma + \Lambda | \qquad (4.18)$$

Hund's Case (a) is appropriate when strong coupling exists between the electronic orbital and spin motion, and the internuclear axis. At the same time electron motion is weakly coupled to the rotation of the molecule. This situation is completely analogous to a symmetric top. The electron motion around the two nuclei results in a non-zero moment of inertia about the internuclear axis. The molecule will precess about the total angular momentum vector J, just as the symmetric top does. The symmetric top is shown in Figure 4.06. The curved arrow in the figure represents the rotation of the entire molecular system about the J vector. Λ indicates the orbital angular momentum of the electrons about the internuclear axis. N is the component of the total angular momentum perpendicular to the internuclear axis.

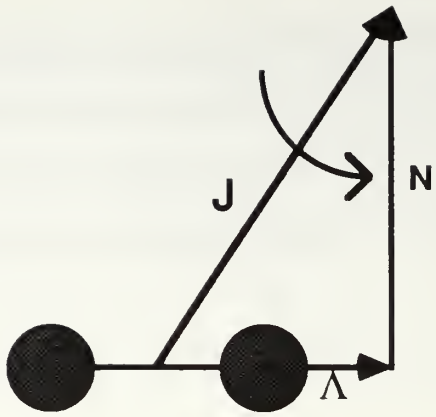

Vector Diagram for a symetric top

Figure 4.06 The Symmetric Top (Herzberg, 1950)

The system in Hund's Case (a) has been complicated by the interaction of the spin and orbital electronic motion with the nuclear rotation and with the internuclear line. The $^1\Sigma$ ground state, where spin and orbital angular momentum go to zero, will be of the same configuration as the symmetric top. Figure 4.07 illustrates the coupling in Hund's case (a). In case (a) the nuclear rotation and electronic motion coupling is weak, while the coupling between electronic motion and the internuclear line is strong. The magnitude and direction of the J vector is constant, while the electronic angular momentum Ω and the angular momentum of nuclear rotation, N, couple to produce the nutation about the total angular momentum J. Additionally L and S are precessing much faster than the precession about J. The bold arrow in Figure 4.07 indicates the nutation of the system about J while the ovals at the end of the Λ and Σ vectors indicate the more rapid precession of L and S about the internuclear line.

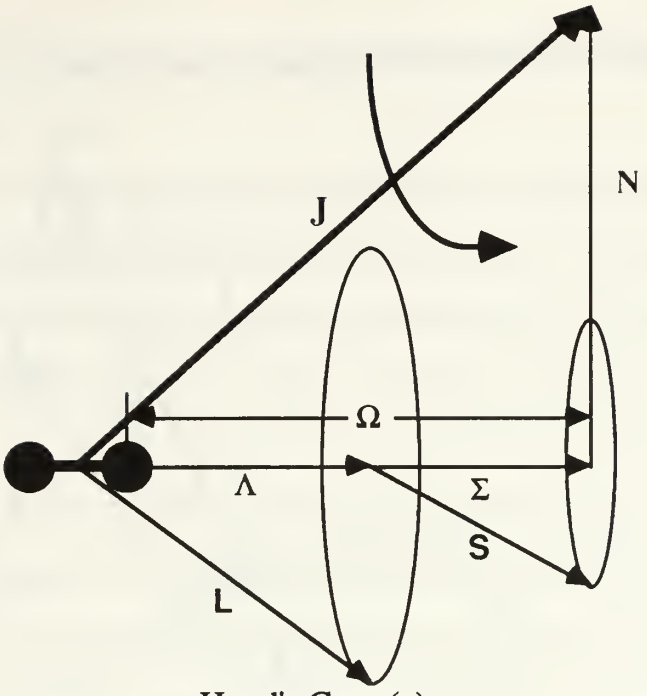

Hund's Case (a)

Figure 4.07 Hund's Case (a) (Herzberg, 1950)

Hund's case (b) has a substantially different coupling scheme. The spin S is only weakly coupled to the internuclear axis. The orbital part of the electronic motion is still strongly coupled to the axis but more moderately coupled to the rotational motion. Additionally, when $\Lambda \Rightarrow 0$ case (a) can no longer apply. The K vector encompassing the total angular momentum apart from spin is then introduced. K is a quantum number with integral values as defined below:

$$K = \Lambda,\ \Lambda + 1,\ \Lambda + 2,\ \ldots \qquad (4.19)$$

The total angular momentum J now follows from 4.19 as

$$J = K + S,\ K + S - 1,\ K + S - 2,\ \ldots\ |\ K - S|. \qquad (4.20)$$

The system configuration and relative coupling for Hund's Case (b) are given in Figure 4.08.

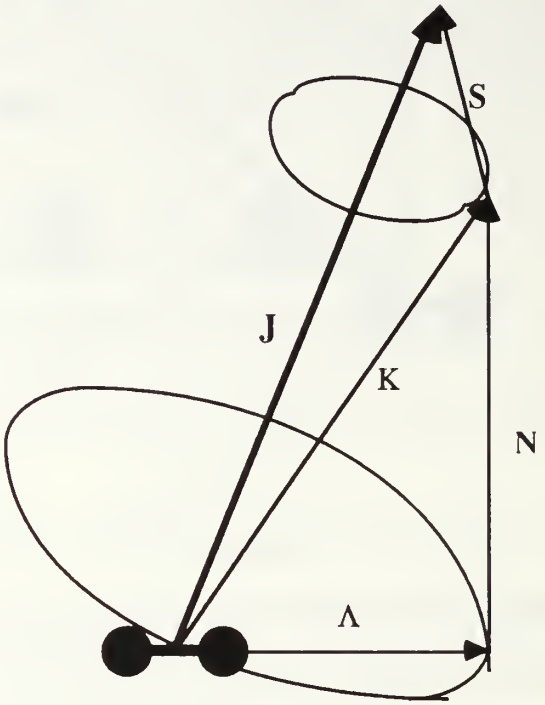

Hund's Case (b)

Figure 4.08 Hund's Case (b) (Herzberg, 1950)

The amount of splitting of the energy levels of a multiplet state depends on the molecule's adherence to Hund's case (a) or case (b). A general rule is that multiplet splitting is large for Hund's case (a) and approaches zero for Hund's case (b). The amount of splitting can be accounted for by the expression

$$T_e = T_0 + A\Lambda\Sigma \,. \qquad (4.21)$$

In equation 4.21 Λ and Σ are as have already been defined and A is a molecular constant for the particular muliplet term.

The Hund's coupling cases discussed above are idealized limiting cases. In general coupling does not neatly comply with one case or another. As rotational energy levels increase, a transition between case (a) and (b) is observed. This is known as uncoupling and there are two types of uncoupling mechanisms between case (a) and (b). These are

Λ-type doubling and spin-type uncoupling. Both mechanisms will cause an energy level splitting. Λ-type doubling occurs for Hund's case (a) and (b), for $\Lambda \neq 0$ states (Π, Δ, Φ etc.). This doubling is very small relative to the other energy differences involved in a transition. Figure 4.09 illustrates Λ-type doubling for two $^2\Pi$ states. The splitting steadily increases as J increases.

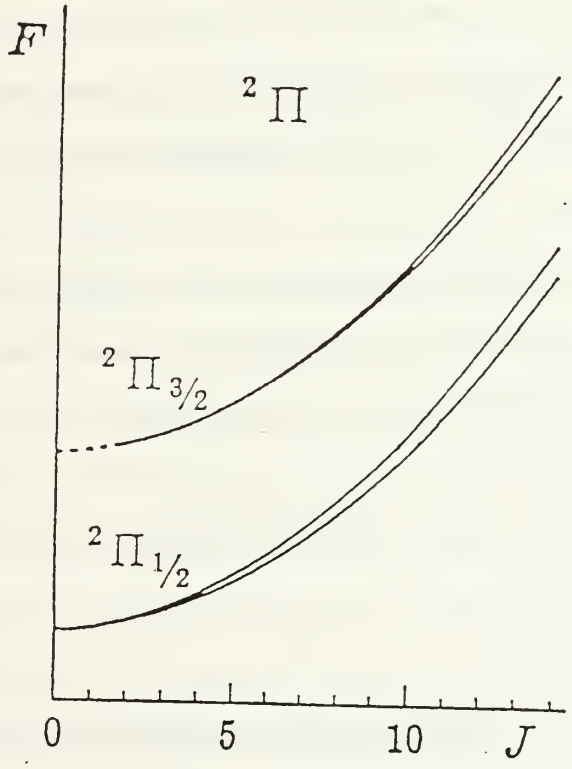

Figure 4.09 Λ-type Doubling for the $^2\Pi$ State (Herzberg, 1950)

Spin-type doubling depends on the spin S for the molecule. As rotational speeds increase, the rotational speed becomes comparable to the precession of S about L. Hund's case (a) is dominant for small rotations and splitting is large. For large rotation the situation approaches Hund's case (b) and splitting is reduced. The result of this larger splitting due to spin-type uncoupling results in different rotational term values for different spin sub-states.

3. Molecular State Populations

The calculation of the population of a specific molecular state requires accounting for all factors that contribute to the population. These factors vary between Hund's case (a) and (b). A state in Hund's case (a) is defined by n, v, and Σ, while case (b) is defined by n, v, and N. For those states where $\Lambda>0$, Λ-type doubling introduces a parity quantum number p that must be accounted for. Although line positions are not sensitive to Λ-type doubling, the calculation of the the population rate and transition probability requires the two sub-states be considered. This is because each Λ-doubled component is individually populated. Transitions from each upper Λ-doubled state constitute a fully resolved line.

The volume emission rate can be calculated by considering the fractional population of the upper state multiplied by a spontaneous emission coefficient between the two states. This is shown for Hund's case (b) in the equation below:

$$E(n'v'N'J'p',n''v''N''J''p'') = N(n'v'N'J'p') \; A(n'v'N'J'p',n''v''N''J''p''). \quad (4.22)$$

where E is the volume emission, N is the fractional population, and A is the Einstein coefficient for spontaneous emission between two states. The factors enclosed are

parameters defining the electronic state n, the vibrational level v, the rotational level N, the vector J, and the parity p. For Hund's case (a) the parameter Σ would replace the rotational level N.

The number of molecules in a specific n' and v' level may be accounted for by the production rate divided by the loss rate in the steady state using

$$N(n'v') = \frac{P(n'v')}{\sum_{v''} A_{v'v''}} . \quad (4.23)$$

Now Equation 4.22 can be multiplied by 1 in the form of N(n'v')/N(n'v') and expressed as

$$E(n'v'N'J'p',n''v''N''J''p'') = P(n'v')\frac{N(n'v'N'J'p')}{N(n'v')}\frac{A_{J'J''}}{\sum_{v''} A_{v'v''}} . \quad (4.24)$$

In equation 4.24 the factor $A_{J'J''}$ is equal to A(n'v'N'J'p',n''v''N''J''p'').

The production mechanism leading to emission for allowed transitions is photoexcitation. The production rate P(n'v'), is proportional to the solar flux and effective cross section for the transition to a specific electronic state. It is assumed that the upper state rotational population is statistically similar to that of the ground state. The branching ratio into various vibrational levels are given by the Frank-Condon factors. These factors arise from the Frank-Condon principle. A brief description of the principle follows. The line strength for a particular transition is a function of the relative positions of the wave functions between the upper and lower states. The electronic transition time for a molecule is on the order of 10^{-16} seconds. Because the vibrational transition time of 10^{-14} seconds is relatively long the internuclear distance will remain virtually constant during the electronic transition. Referring back to Figure 4.04, this transition may be expressed as a

vertical line between electronic states. The maximum probability density in the excited state will determine the upper state location. A strong wave function spatial overlap will determine the most likely lower eigenstate. The most favored location is generally at the end of an oscillation where the eigenfunction is a maximum. The relative strength of a transition from a vibrational level (v') of an excited electronic state to the vibrational level (v") of a lower electronic state is then based on the locations of the upper and lower levels, and the probability amplitude at the respective upper and lower locations. This concept, is known as the Frank-Condon principle (Eisberg, 1985).

The production rate for an allowed transition can be written as

$$P(n',v') = \pi F \frac{\pi e^2}{mc^2} \lambda^2_{ov'} f_{xn'} q_{ov'} \qquad (4.25)$$

where πF is the solar flux (photons cm^{-2} $sec^{-1}Å^{-1}$), λ is the wavelength of incoming radiation, $f_{xn'}$ is the oscillator strength for the electronic transition from the ground state to the n' state, and $q_{ov'}$ is the Frank-Condon factor between the v=0 level of the ground state and the v' level of the upper n' state. This production equation makes the valid assumption that virtually all molecules are in the ground state prior to absorbing incident radiation.

Tatum (1967) develops a detailed description to determine the relative populations of molecular energy levels. The development is summarized here. The fractional population $\frac{N(n'v'N'J'p')}{N(n'v')}$ of a given state generally obeys a Boltzman distribution. The Boltzman distribution for a state can be expressed as

$$\frac{N_i}{N} = = \frac{g_i e^{-E_i/kT}}{\sum_j g_j e^{-Ej/kT}} . \qquad (4.26)$$

In Equation 4.26, g_i is the statistical weight of the ith group and the denominator is the associated partition function. Tatum applies this distribution to the different molecular sub-states corresponding to appropriate Hund's coupling cases. As an example for Hund's case (b) in states where $\Lambda \neq 0$, the fractional population may be expressed as

$$\frac{N(n'v'N'J'p')}{N(n'v')} = \frac{hc\ B_v}{kT}\,\Phi\,\frac{(2J+1)}{(2S+1)}\exp\left(\frac{hcF(N)}{kT}\right) . \qquad (4.27)$$

The factor Φ introduced in Equation 4.27 is a constant for hetero- or homo- nuclear molecules. The various other factors in equation 4.27 have all been defined previously. A similar expression is obtained for Hund's case (b).

The remaining factor in equation 4.24 $\dfrac{A_{J'J''}}{\sum_{v''} A_{v'v''}}$, is yet to be determined.

The factor $A_{J'J''}$ is the transition probability. This probability for the rotational branching between two vibrational levels can be determined by the Honl-London factors. These factors sum to the value 2J +1 so in order to normalize the factor it must be divided by 2J +1. This will yield the correct branching probability. The Honl-London factors yield the probability of a rotational branch for a given v'-v" transition. To consider a transition on the specific v" level another factor $A_{v'v''}$ must be included. The factor $A_{J'J''}$ becomes

$$A_{J'J''} = A_{v'v''}\,\frac{S(J'J'')}{2J'+1} . \qquad (4.28)$$

Equation 4.24 can now be rewritten as

$$E(n'v'N'J'p',n''v''N''J''p'') = \frac{N(n'v'N'J'p')}{N(n'v')}\,\frac{A_{v'v''}}{\sum_{v''} A_{v'v''}}\,\frac{S(J'J'')}{2J'+1} . \qquad (4.29)$$

The single-scatter albedo $\varpi_{v'v''}$ of a fluorescent band is defined as

$$\varpi_{v'v''} = \frac{A_{v'v''}}{\sum_{v''} A_{v'v''}} \quad . \qquad (4.30)$$

The factor $A_{v'v''}$ is the transition probability of a molecular band which is related to the band strength by the relation shown below:

$$A_{v'v''} = \frac{64\pi^4 \nu^3_{v'v''}}{3hc^3 \; d_{v'}} \; Re^2 \; q_{v'v''}. \qquad (4.31)$$

In Equation 4.31 $\nu_{v'v''}$ is the frequency of the band, $d_{v'}$ is the degeneracy of the upper level and $Re^2 \; q_{v'v''}$ is a close approximation of the band strength $S_{v'v''}$. These factors allow Equation 4.28 to be expressed as

$$\tilde{\omega}_{v'v''} = \frac{\nu^3_{v'v''}}{\sum_{v''} \nu^3_{v'v''} q_{v'v''}} \quad . \qquad (4.32)$$

Equations 4.30 through 4.32 can now be substituted into Equation 4.29 to yield the volume emission rate.

Production for forbidden transitions conforms to the required calculations for electron impact excitation. The relative speed and abundance of electrons in the ionosphere results in collisions between electrons and neutral molecules being the dominant production source for forbidden transitions. Excitation by electron impact becomes the

dominant source of the excited state for the transition. The source equation is now highly dependent on the electron flux, as well as the electrons cross section for excitation. The emission rate as compiled by Barth (1965) is given by

$$4\pi I_{v'v''} = \int_{E}^{E_{max}} I_E \sigma_E \, dE \;\; q_{ov'} \, \tilde{\omega}_{v'v''} \, N_0 \;\; ch(\theta) \qquad (4.33)$$

where I_E is the particle flux in electrons cm^{-2} sec^{-1}. Both, the electron particle flux and the electron cross section for excitation of an electronic state σ_E are energy dependent. The Franck-Condon factor for excitation $q_{ov'}$, single-scattering albedo $\tilde{\omega}_{v'v''}$, and molecular column density N_0, adjusted by the Chapman function $ch(\theta)$, remain consistent with those for the photoexcitation case. It is necessary to integrate over all available electron energies when a range of electron energies is present. This is the usual case in the ionosphere.

The methods of this section have been used to compile the synthetic spectra to be illustrated in Chapter V. Each spectrum is highly dependent on the unique properties of each molecule involved. Separate algorithms have been used for each emission feature in Chapter V. The actual calculation requires that a volume emission rate for each line in the band be calculated. The contribution from each bin is then summed to produce the spectrum. An example of this process is shown in Figure 4.10. In this figure the (1,0) gamma band of Nitric Oxide is shown for a wavelength bin size of .03 Å. The individual lines are distinct. The spectra in Chapter V have a lower resolution comparable to instrument resolving capability. As a result individual rotational lines are not distinguishable.

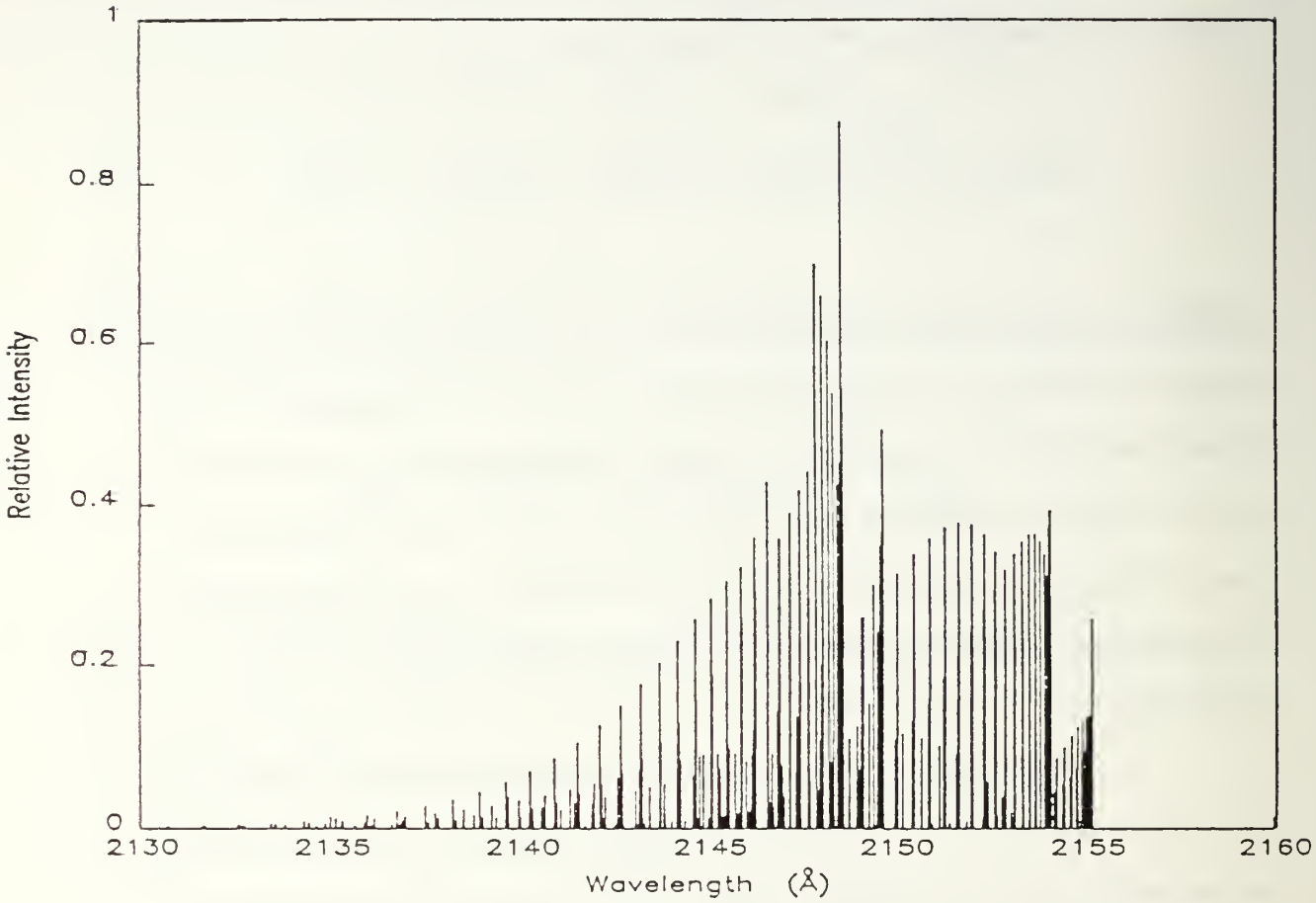

Figure 4.10 Synthetic Spectrum for (1,0) Gamma Band Emissions (Cleary, 1985)

V. DAY GLOW EMISSION FEATURES IN THE 1800-3400 Å WAVELENGTH RANGE

This chapter is concerned with identifying observable emission features in the wavelength range of the instrument. N_2, O_2, O and NO all have emissions in the 1800-3400 Å window. The transitions result from the interactions presented in Chapter IV. There are additional emission bands that occur in the window besides those that will be described. These are of such a low intensity at the altitudes of interest that they are not measurable. The bands and lines presented in this chapter are primarily the ones that are predicted to be observed, during the flight. Computer simulations of synthetic spectra have been created by McCoy (1981), Cleary (1985), and Conway (1982).

The observed intensity will be limited by the detector efficiency. The instrument detector efficiency is limited at the long end of the experimental wavelength range by photocathode efficiency. Figure 5.01 shows this efficiency over the wavelength range of the instrument. The solid curve in the figure demonstrates that detector efficiency drops off rapidly past 3000Å . This efficiency drop will become a significant consideration when attempting to identify emission features of longer than 3000Å that are observable.

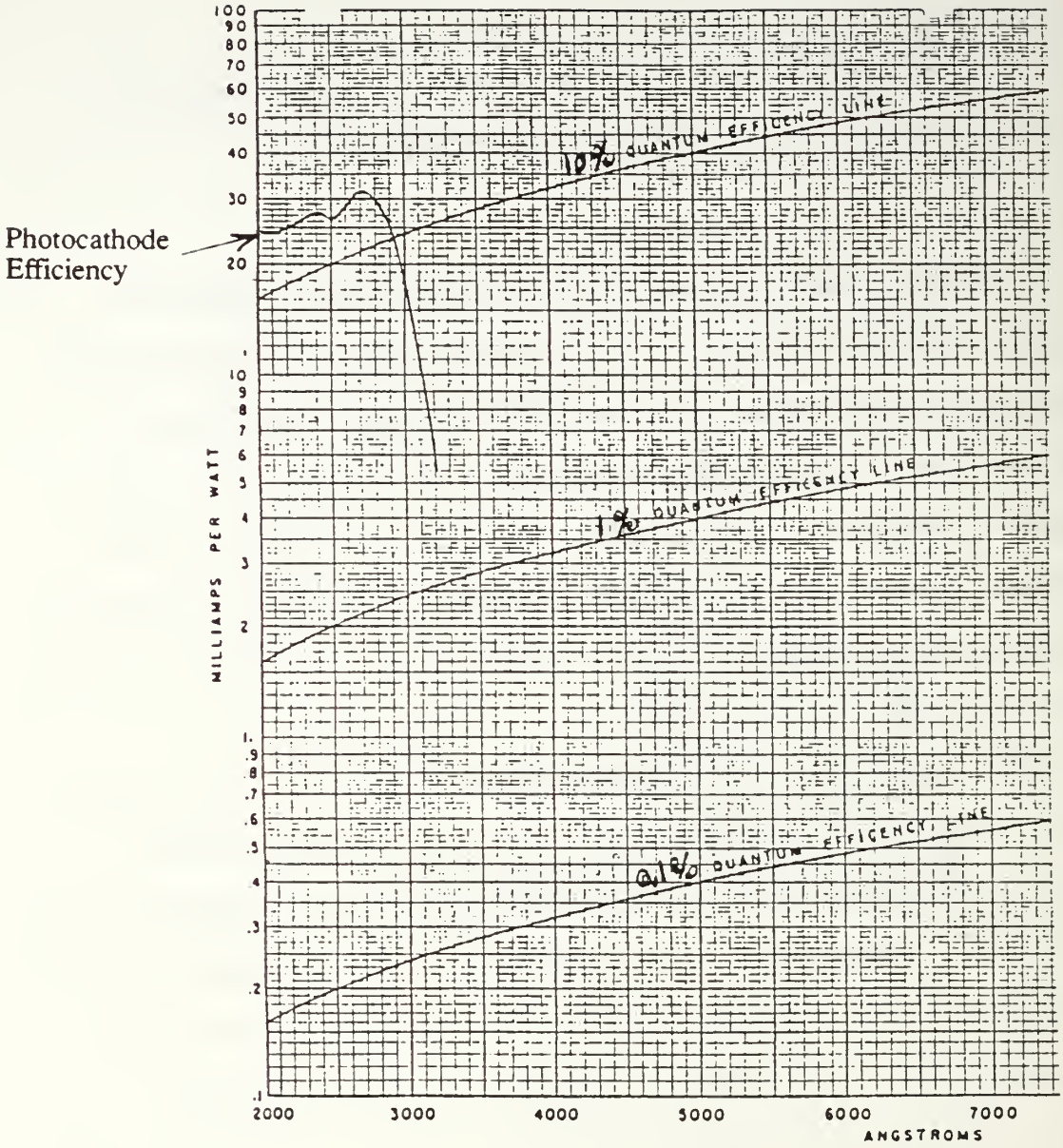

Figure 5.01 Photocathode Efficiency

A. MOLECULAR NITROGEN

Molecular nitrogen has three observable band systems: the Vegard-Kaplan ($A^3\Sigma_u^+ - X^1\Sigma_g^+$), 2nd positive ($C^3\Pi_u - B^3\Pi_g$), and the Lyman-Birge-Hopfield ($a^1\Pi_g - X^1\Pi_g$) bands. The Birge-Hopfield ($b^1\Pi_u - X^1\Sigma^+_g$) band was also investigated as a possible

contributor but its intensity in the experimental window was found to be negligible. The potential energy curves for N_2 are shown in Figure 5.02. References to specific energy levels of the N_2 molecule will be from this figure. In addition, Figure 5.03 is a schematic energy level diagram of N_2. This figure illustrates the major transitions of molecular nitrogen. It also displays the relative energy differences for the emission bands.

It is of note that molecular nitrogen is the dominant component of the atmosphere at the lower end of the experimental altitude range. However, at around 175 km atomic oxygen becomes the dominant species (see Figure 2.08). Since N_2 is the dominant species, a reaction involving N_2 may be observable although it has a relatively low emission probability. Additionally, the relative importance of N_2 is strongest at lower altitudes and will tend to drop as altitude increases unless some other factor arises such as quenching at lower altitudes. The N_2 emissions in the ultraviolet tend to be weak because they are a result of forbidden transitions subject to quenching, or a combination of both factors.

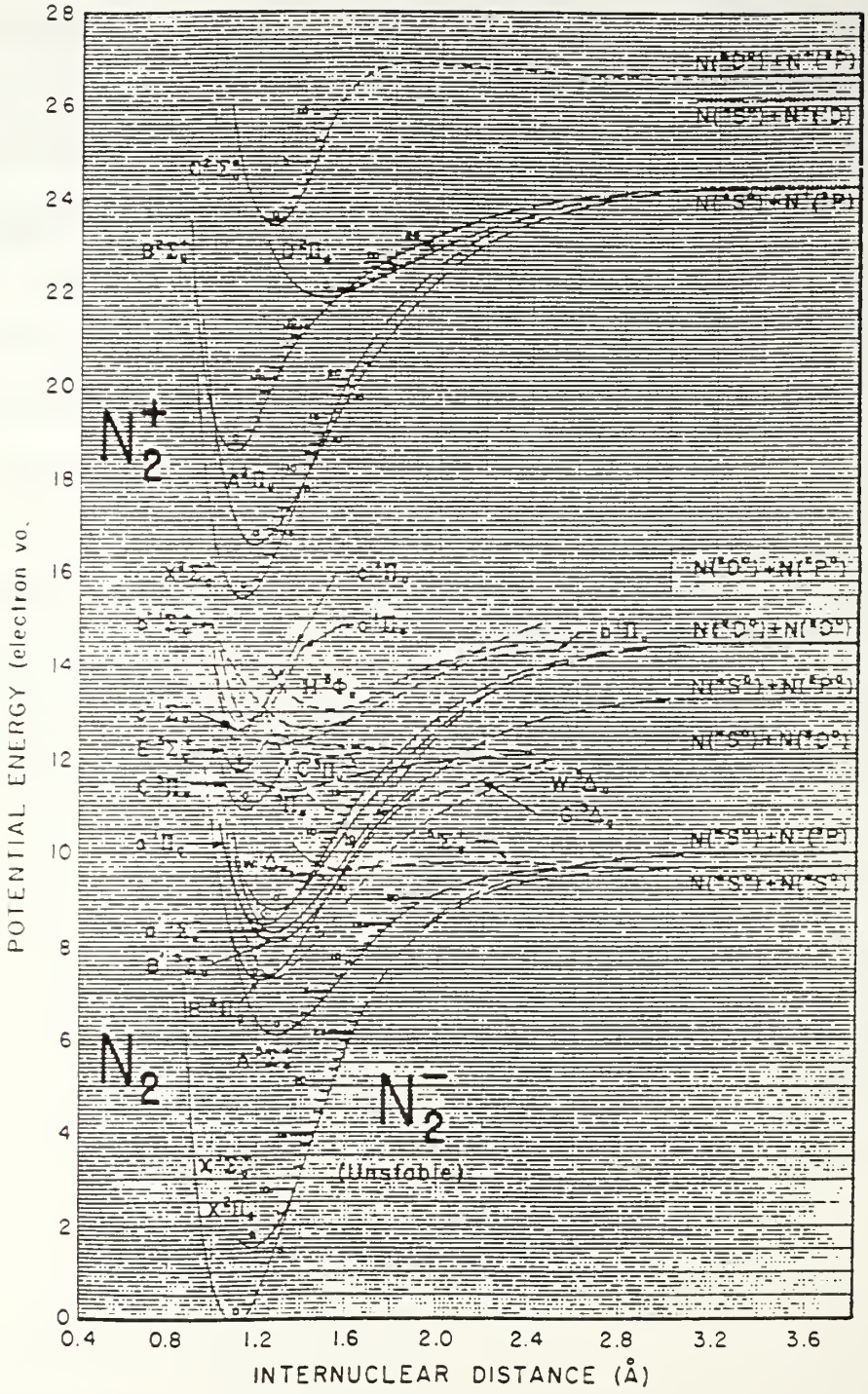

Figure 5.02 N_2 Potential Energy Curve

(Journal of Physical Chemistry Reference Data, 1977)

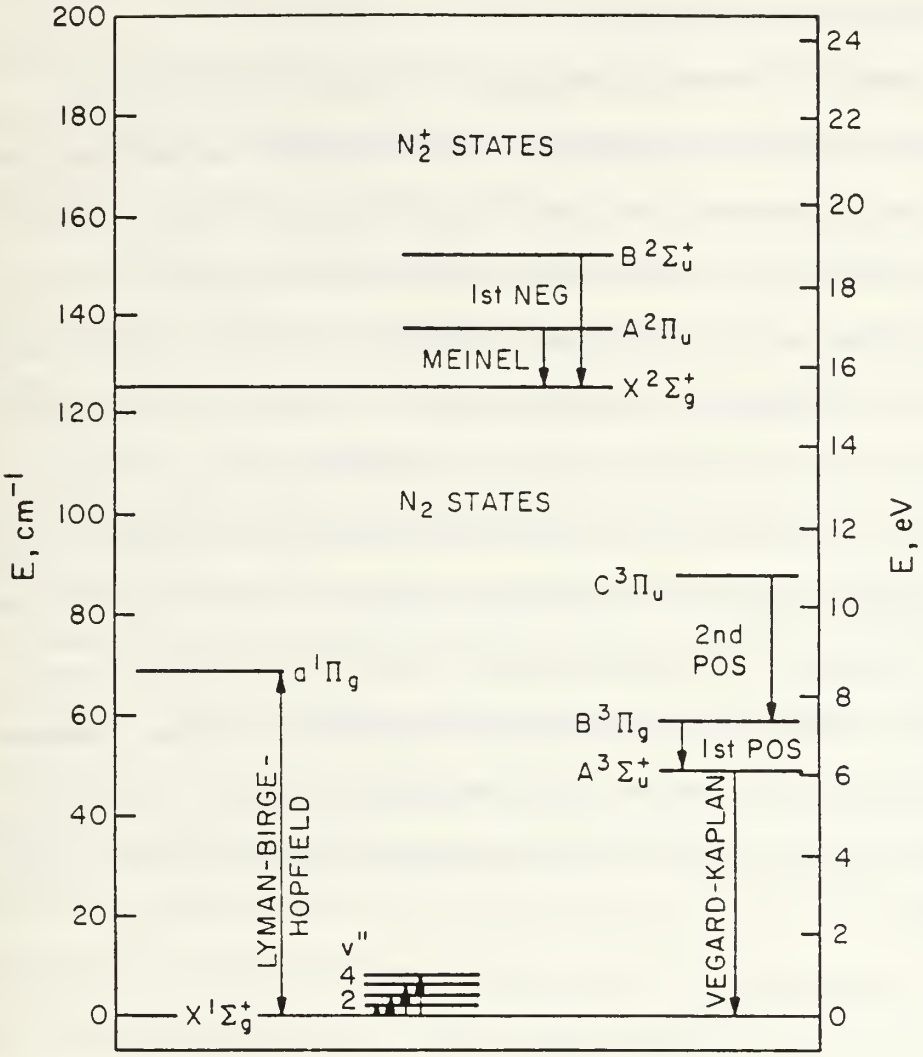

Figure 5.03 N_2 Energy Level Diagram (Sharp, 1970)

1. Vegard-Kaplan System

The V- K system represents the $A^3\Sigma_u^+ - X^1\Sigma_g^+$ transition, and has a range of 1250 to 5325Å (Krupenie, 1977). In 1932, Vegard first discovered the system by bombarding solid nitrogen with electrons. Later in 1934, Kaplan succeeded in obtaining

V-K bands with gaseous nitrogen. Kaplan also adjusted the wavelengths of the lines proposed by Vegard. (Krupenie, 1977)

Barth (1965) identified both fluorescence and electron processes as production sources for the V-K emissions. However, Sharp (1970) has determined that the sources for the upper state are almost exclusively due to electron impact. The upper state $A^3\Sigma^+_u$ is populated as a result of direct excitation by electron impact, as well as cascading from higher states (Broadfoot and Hunten,1964). Dominant sources of cascade are directly from the $B^3\Pi_g$ state and indirectly from the $C^3\Pi_u$ state. It is of note that the relative population of the vibrational levels depends on the excitation source. Table 5.01 has been computed to demonstrate the relative distribution of vibrational levels as a result of each case. The first row considers the distribution for direct excitation to the $A^3\Sigma^+_u$ state. The second row considers the relative distribution of vibrational states only for cascade from higher states. While direct excitation results in a concentration at higher vibrational levels, cascade results in a concentration at the lower vibrational levels. Table 5.01 is in non-normalized units where a larger number indicates a higher relative population of the entire $A^3\Sigma^+_u$ state.

TABLE 5.01

RELATIVE POPULATIONS OF THE $A^3\Sigma^+_u$ STATE

(Ahmed, 1969)

v'	0	1	2	3	4	5	6	7	8	9	10
direct	.15	1.0	2.75	6.0	10.25	15.25	19.5	22.75	24.75	25	24
cascade	.95	1.0	.78	.57	.35	.19	.09				

This scheme is further complicated by the proposal by Campbell and Thrush (1967) and later by Gilmore (1969) that inverse first positive transitions act as non-radiative loss mechanisms (see Figure 5.03). It has been suggested by Torr and Torr (1982) that the complex population mechanisms for the V-K system require further data. This experiment may be able to provide some useful data at the upper end of the experimental altitude range.

Because the upper state of the Vegard-Kaplan state is metastable, quenching rather than emission will dominate. This is particularly true at the low altitude end of the experiment. It has been shown that the Vegard-Kaplan band is a weak feature in the dayglow although it is quite bright in the aurora (Torr and Torr, 1982). The primary reason for this appears to be quenching. Shemansky (1969) determined that the upper state possessed a mean lifetime of 1.8 seconds. The atmospheric collision frequency is about 2.25 per second at 120 km (CIRA model 1965, in Sharp, 1970). Therefore at low altitudes there is a likelihood of four collisions prior to an emission. Quenching may result from collisions between N_2 and neutral atoms or molecules. Candidates include N_2, O_2, O, NO, and N as potential quenching agents (Torr and Torr, 1982). Sharp (1970) has identified O as the dominant agent. The number density for all species drops by two orders of magnitude between 100 and 200 km (see Figure 2.08). Collision frequency can be expected to drop off proportionally. Thus, the Vegard-Kaplan bands will assume an increasingly significant role as altitude increases.

Conway (1985) has identified the (0,9) band at 3353Å as having an intensity of 2 kR at an altitude of 150 km. This is a detectable amount although it is well past the 3000Å threshold of reduced detector efficiency. It is necessary to investigate other vibrational bands in the V-K system to determine whether or not this band system will be observable. There is a convenient factor to distinguish the relative intensities of emission bands for a particular band system. This factor is a combination of the Frank-Condon

factor for excitation and the albedo for scattering (Q- omega). This is interpreted as that portion of the total excitation to a particular electronic state that is excited to a specific v' state and emitted back down to a particular v" state. The Q.omega factor for the (0,9) feature is 2.47×10^{-5}. Numerous emission features below the 3000Å cutoff have similar or even higher Q-omega factors (Barth, 1965). The highest is the (5,1) band at 1841Å, with Q-omega equal to 1.48×10^{-2}. This would support the contention that N_2 V-K should be observable in measurable quantities during this experiment.

The V-K transition is spin forbidden but remains electric dipole radiation (Conway, 1980). It violates the $\Delta s = 0$ requirement as the spin 3 to spin 1 states, are not allowed. However,the $^3\Sigma_u^+$ to $^1\Sigma_g^+$ transition will occur despite it being forbidden. Herzberg (1950) states that the spin orbit interaction causes the $^1\Sigma$ state to "borrow" some of the characteristics of the allowed $^3\Pi_0$ state, or the $^3\Sigma$ state "borrows" some of the characteristics of the $^1\Pi$ state. Four branches will result. The synthetic Vegard-Kaplan spectrum between 1800-3400 Å is shown in Figure 5.04.

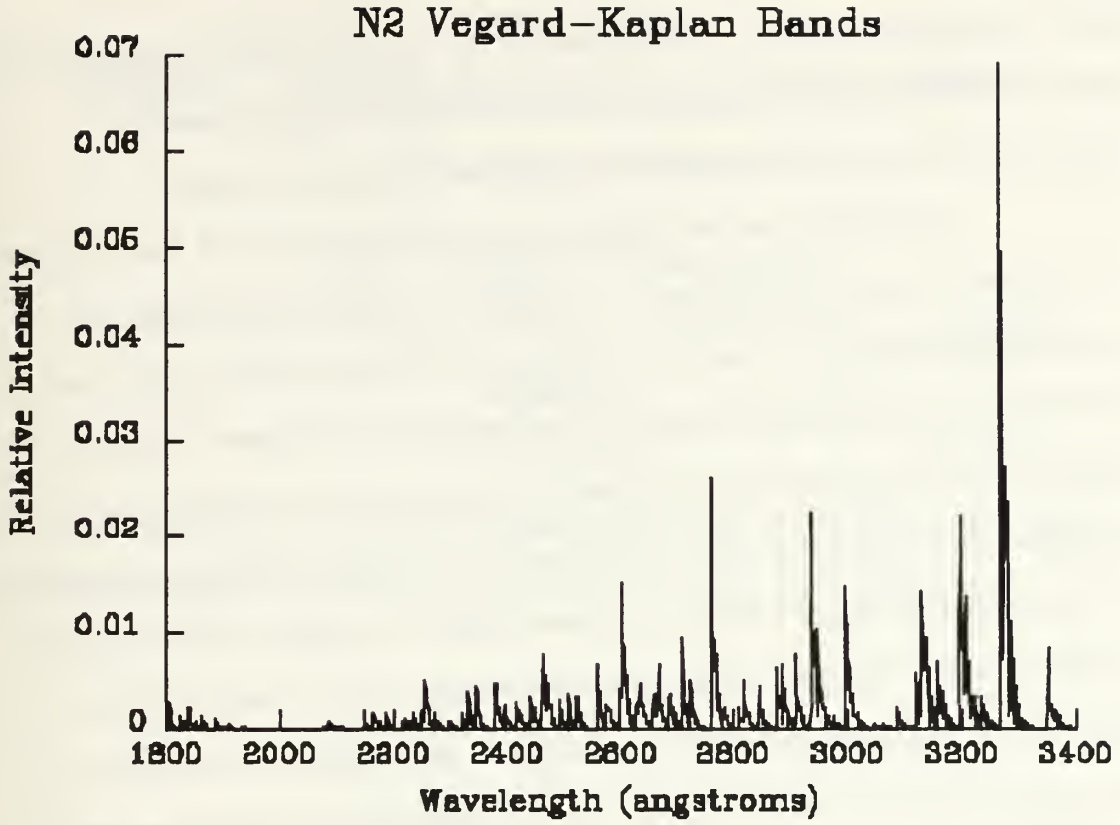

Figure 5.04 N_2 Vegard-Kaplan Bands

2. N_2 Second Positive System

The second positive system represents the $C^3\Pi_u$ - $B^3\Pi_g$ transition. It ranges from 2680 to 5460Å (Krupenie, 1977). The Second Positive system was first observed in 1869 (Krupenie, 1977). It appears in most nitrogen sources including pure nitrogen and air. It was observed in the dayglow as early as 1945 (Pearse and Gaydon, 1963). Numerous observations include a recent experiment by Conway (1980) in 1980.

Conway and Christensen (1985) reported an observed intensity of about 10kR for the (0,0) feature at 3370Å during solar maximum conditions. It appears that this is the brightest feature in the experimental wavelength region. Other features in the region are less intense. The Q-omega factor for the (0,0) band is .280 . The highest factor below

3000Å is the (2,0) with a value of .021 (Barth, 1965). This is an order of magnitude lower than the (0,0) band and is an indication that the 2nd-Positive band will make little contribution to the observed emissions in the experimental wavelength region.

The intensity can be calculated using the following method. From Equation 4.33, the intensity due to electron impact excitation is equal to the product of the total electron impact cross-section, slant column density, and Q-omega factors for the band. The calculation used the electron impact cross-sections for the $C^3\Pi_u$ state which is shown in Figure 5.05. The cross-section at each energy can be multiplied by the electron flux at that energy. The electron flux has been calculated in a simulation by Strickland and Meier (1982) using an F10.7 equal to 206, a solar zenith angle of 56 degrees, and a temperature at infinity of 1000K. The data points on the figure indicate separate results by E. Oran (Oran, 1978). The electron flux at each energy can be multiplied by the cross-section at each energy the result is shown in Figure 5.07. The integration over the electron energy range shown in Figure 5.07 will yield the total electron excitation cross-section for each state. This cross-section multiplied by the Q-omega factor and a representative column density at a given altitude will give the expected observable intensity in Rayleighs. The slant column density is computed by adjusting the vertical column density by the chapman function for looking across the limb. This has been done for the values given in Table 5.02.

TABLE 5.02

INTENSITY FACTORS FOR $N_2(C^3\Pi_u - B^3\Pi_g)$ TRANSITION

$$\int_{E}^{E_{max}} \sigma_E I_E \, dE = 8.25 \times 10^{-9}$$

$q_{0v'\omega_{v'v''}}$ (Q-omega) = .28 (Barth, 1965)

$N = 1.8 \times 10^{18}$ mol cm^{-2} {for N_2 n(150km) = 1.0×10^{10} mol cm^{-3}, t_{inf} = 1800°K, ch(30,90°)}

$4 \pi I = 4.2$kR

This calculated intensity is a reasonable approximation to the measured value of 10kR, considering that both N_2 column densities and electron fluxes are approximated.

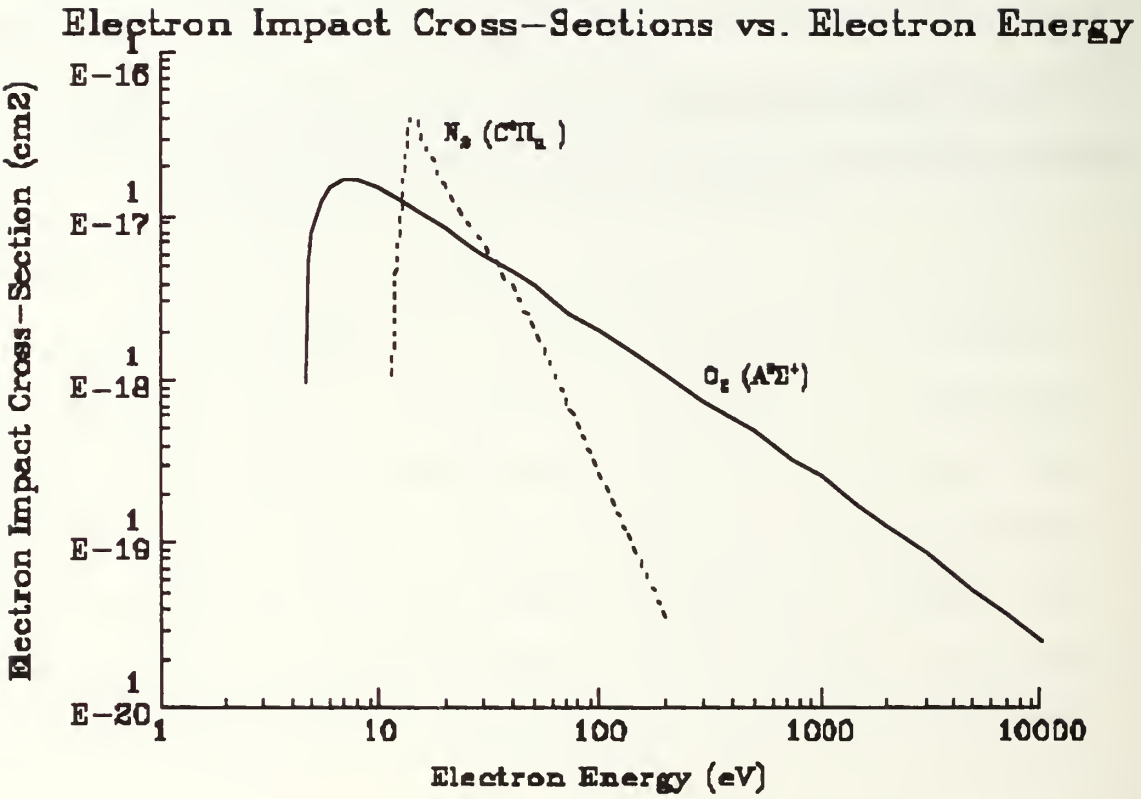

Figure 5.05 Electron Impact Cross-Section vs. Electron energy $N_2(C^3\Pi_u)$ and $O_2(A^3\Sigma^+_u)$ states (Cartwright et al, 1977 and Borst, 1972).

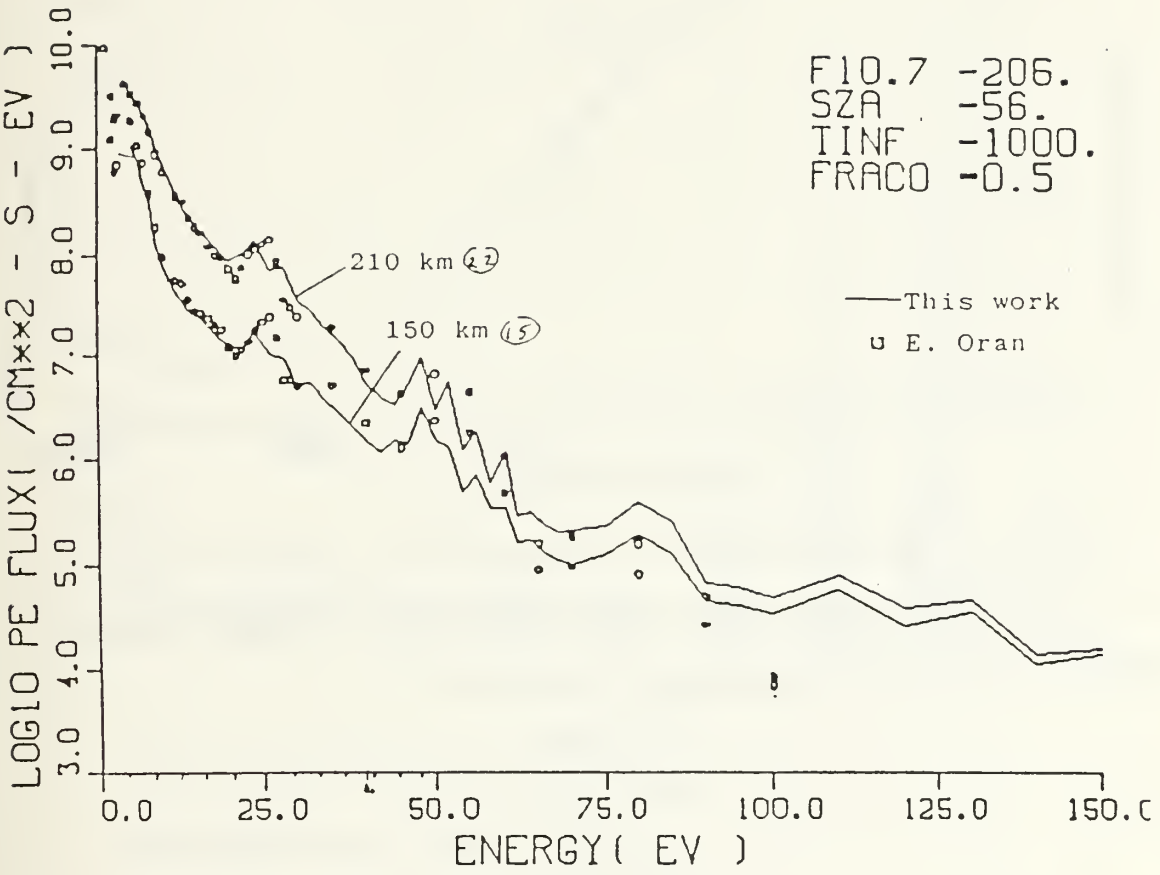

Figure 5.06 Electron Energy vs Electron Flux (Strickland & Meier,1982)

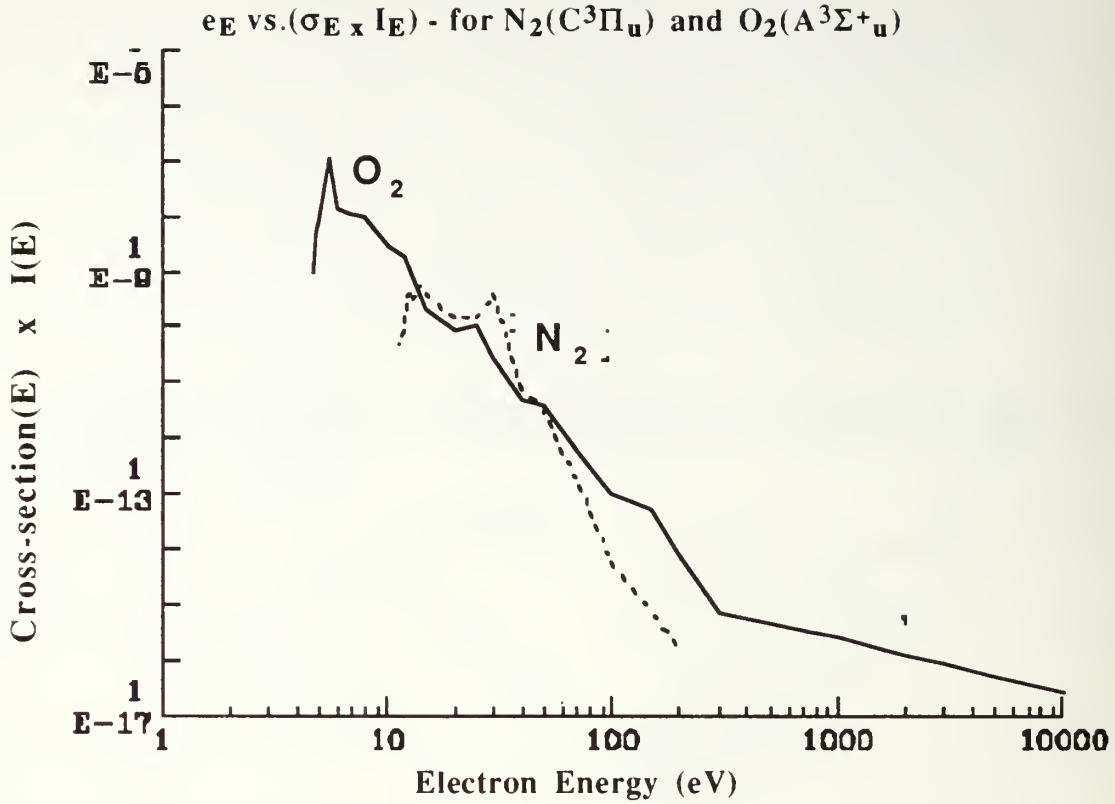

Figure 5.07 Electron Energy vs. (Cross-section x Electron Intensity)

Because of the the $\Delta\Sigma = 0$ selection rule discussed in Chapter V, three sub-bands will result for Hund's case (a)

$$^3\Pi_0 - {}^3\Pi_0$$

$$^3\Pi_1 - {}^3\Pi_1$$

$$^3\Pi_2 - {}^3\Pi_2$$

(Herzberg, 1950). Each sub-band has a strong P and R branch. The Q branch is a weak branch except for the $^3\Pi_0 - {}^3\Pi_0$ case. This results in triple band heads which are degraded to the blue. The Physical Chemistry Reference Data Manual (Krupenie, 1977) has identified fifty of the bands. When J is small, the transition conforms to Hund's case (a) (see Figure 4.07). As J becomes larger, the coupling approaches that of Hund's case (b) (see Figure 4.08). This transition exhibits some Λ-type doubling doubling, as required by

Hund coupling for a $^3\Pi$ - $^3\Pi$ transition. The second positive synthetic spectrum that will contribute to the experimental window is shown in Figure 5.08.

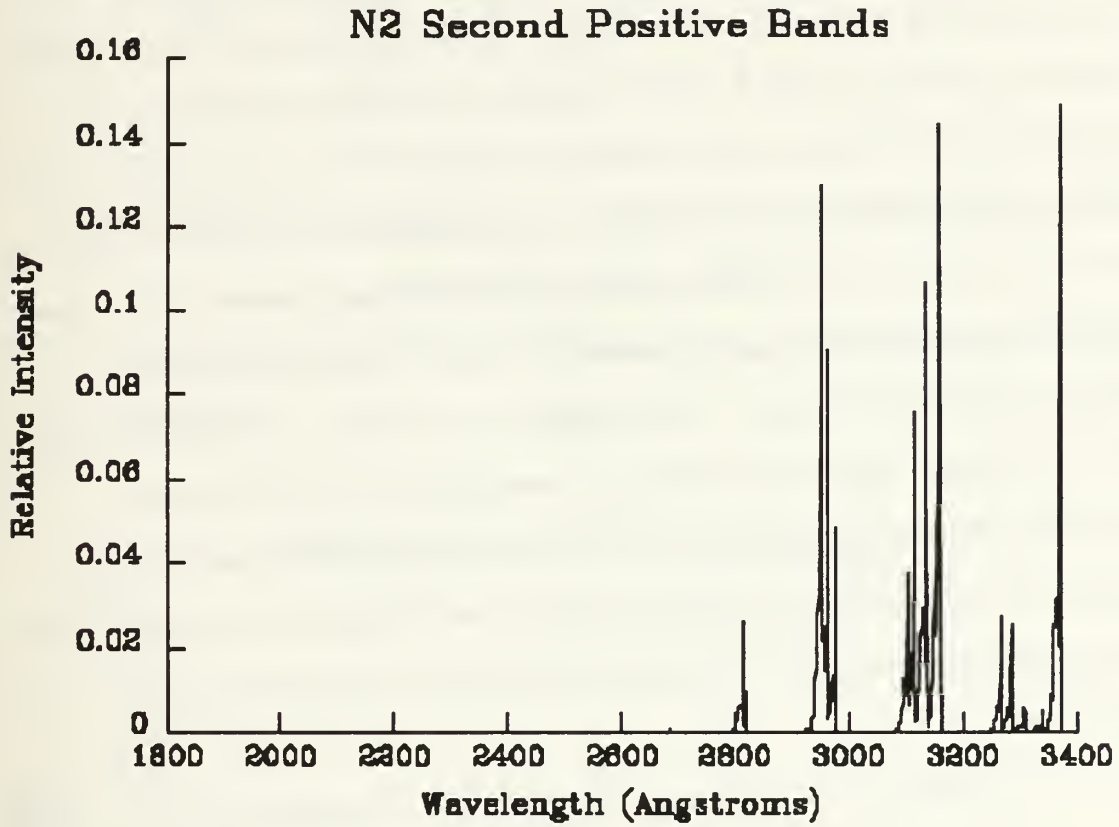

Figure 5.08 N_2 Second Positive Bands

3. Lyman-Birge-Hopfield Band

The Lyman-Birge-Hopfield bands ($a^1\Pi_g$ - $X^1\Sigma^+_g$) have a wavelength range from 1160 to 3020 Å (Barth, 1965). The emission bands were first observed in 1928 by Birge and Hopfield (Pearse and Gaydon, 1963). They are readily visible as both emission and absorption features in the vacum ultraviolet.

The transition is forbidden as electric dipole radiation Emissions will result from electric quadrupole and magnetic dipole transitions. Furthermore, the upper state is

forbidden from the ground state (Herzberg, 1950). The excitation will occur primarily as a result of electron bombardment.

LBH emissions have been used as an accurate measure of the photoelectron flux (Conway, 1982). Conway observed dayglow intensities approaching 800 R at 160 km for the (2,0) feature at 1383 Å. The Q-omega factor for the (2,0) band is 4.63×10^{-2}. The (2,8) band at 1837Å has a Q-omega factor of 1.87×10^{-2}. The (3,9) at 1854Å, (3,10) at 1928Å, (4,10) at 1870 and (4,11) at 1945Å emission bands all have similar Q-omega factors; on the order of 10^{-2} [see Barth (1965) for the complete table electron impact cross-sections]. This would indicate that LBH emissions should be visible in measurable intensities in the wavelength region. These features are at the short wavelength end of the detector which has a relatively low efficiency . Nevertheless, it would seem that the Lyman-Birge-Hopfield Bands should contribute to the observed experimental intensity. The peak observed intensity for all LBH emission features should be in the range of 150 to 200 km in altitude if atmospheric conditions during Conway's observations remain generally in effect.

The $a^1\Pi_g - X^1\Sigma^+_g$ transition violates the $g \Leftrightarrow u$ selection rule given in Table 5.1. The transition is allowed by the special selection rules of Table 5.2. The ΔJ selection rule for quadrupole radiation becomes

$$\Delta J = 0, \pm 1, \pm 2 \text{ (Herzberg, 1950).}$$

The resultant branch structure is some what complicated. It is best presented graphically as is shown in Figure 5.09.

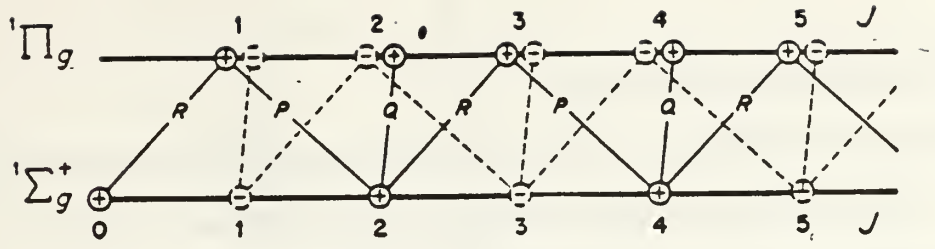

Figure 5.09 Π_g - $^1\Sigma^+_g$ Branches for Magnetic Dipole and Quadrupole Bands (Herzberg, 1950)

The branch structure of the LBH system will produce the lines shown in Figure 5.10 in the experimental window.

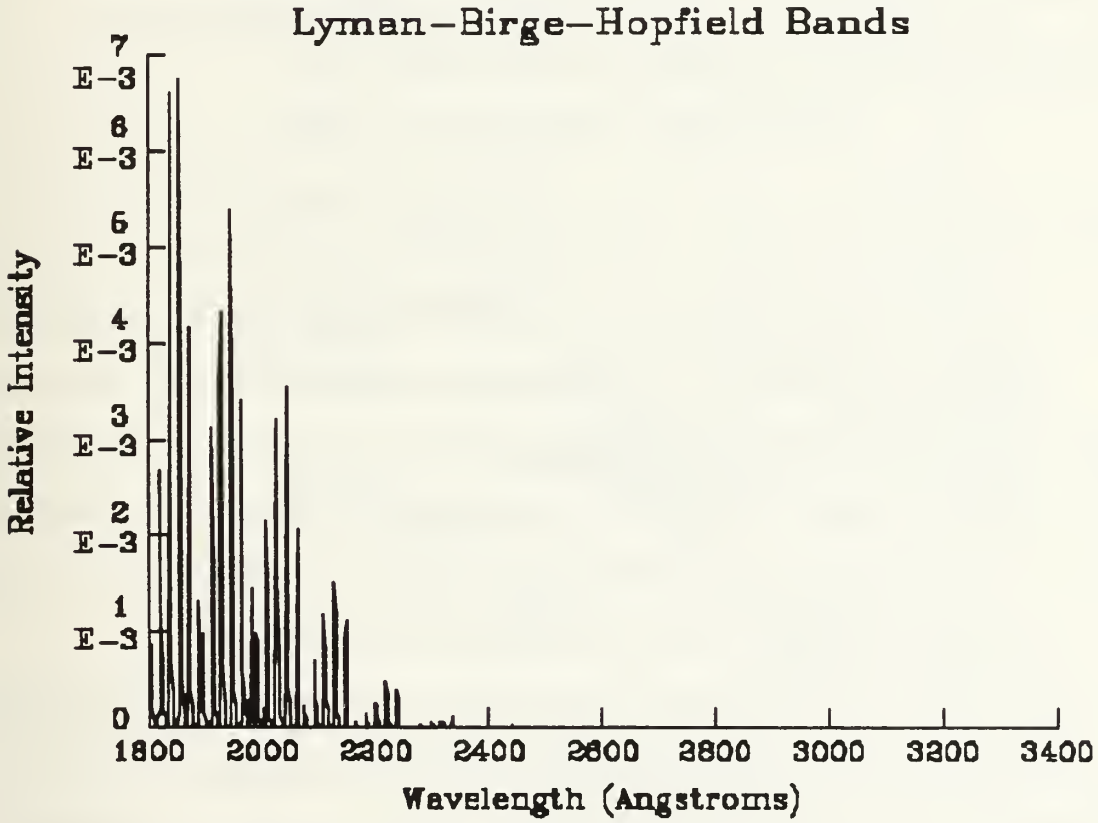

Figure 5.10 N_2 LBH Bands (Cleary, 1985)

B. MOLECULAR OXYGEN

There are two observable bands of O_2 that may contribute to the experimental window. These are the Herzberg I, and Schumann-Runge (SR) bands. The first of these is forbidden, while the second is an allowed transition. The potential energy level diagram for O_2 is shown in Figure 5.11. The schematic energy level diagram for O_2 is shown in Figure 5.12. This figure demonstrates the major transitions of molecular Oxygen. It also displays the relative energy differences for the emission bands.The Schumann-Runge bands have an easily accessible threshold energy for photo dissociation which minimizes the observed intensity. The energy curve for the $B^3\Sigma^-_u$ is of note. This is the upper state for the Schumann-Runge transition. O_2 in this state will dissociate into $O(^3P) + O(^1D)$ atoms. It may also predisscociate to the $O(^3P) + O(^3P)$ atoms. The upper state for the Herzberg system ($A^3\Sigma^+_u$) may also result in the $O(^3P) + O(^3P)$ atoms.

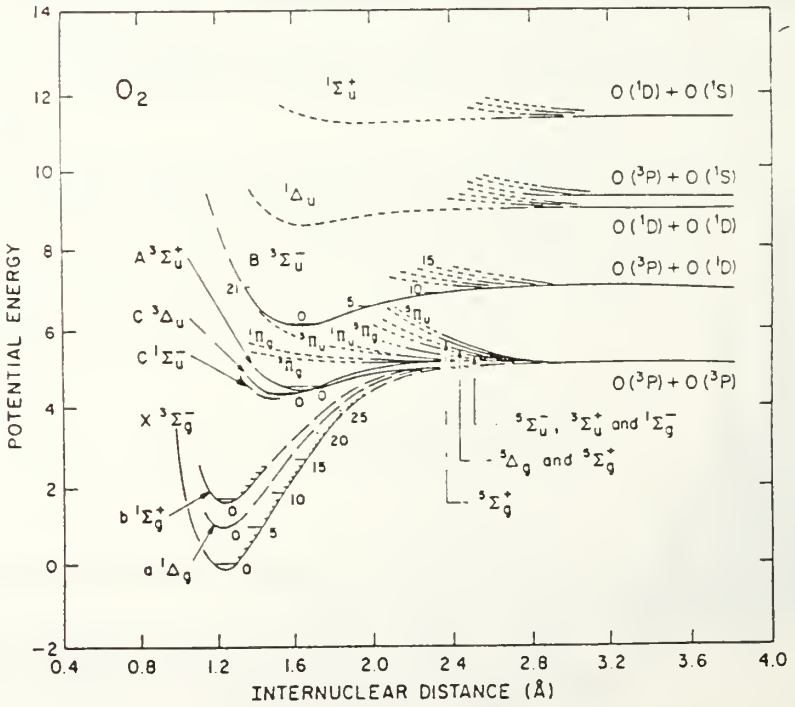

Figure 5.11 O_2 Potential Energy Diagram (from Gilmore, 1965)

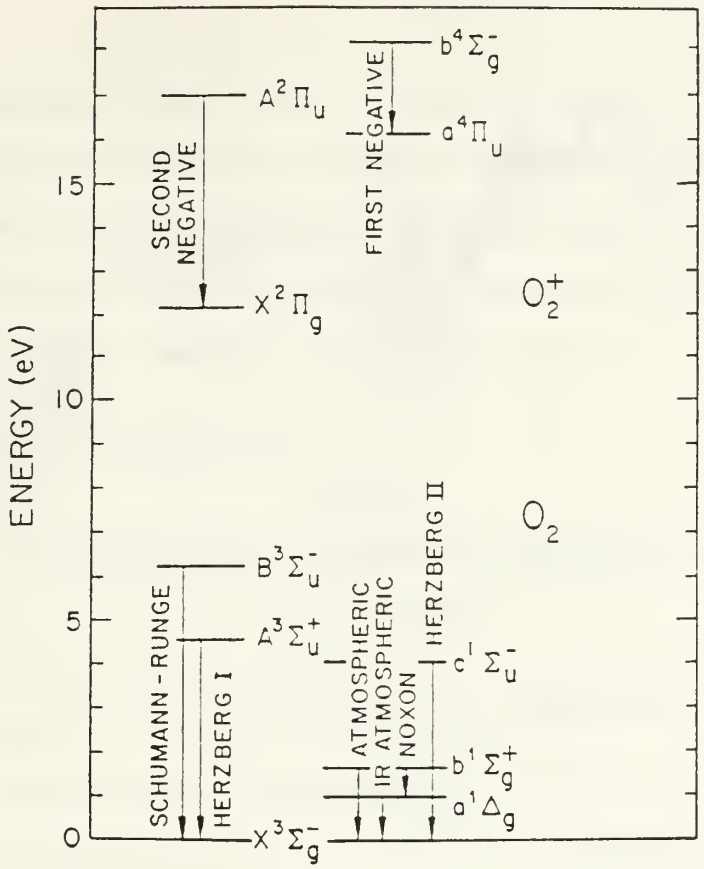

Figure 5.12 O_2 Energy Level Diagram

1. Schumann-Runge Bands

The Schumann-Runge system ($B^3\Sigma^-_u$ - $X^3\Sigma^-_g$) ranges from 1750 to 5350 Å. With over 100 single-headed red degraded bands, the Schumann-Runge (SR) is a very extensively studied Oxygen system. It was identified by Schumann as early as 1903 (JPCRD, 1972).The large number of lines arises from the greater internuclear distance of the upper electronic state over the lower state. This results in a large number of accessible lower vibrational levels for each upper vibrational level.

The $B^3\Sigma^-_u$ state has a strong absorption cross section However as mentioned above, this state lies very close to the Oxygen dissociation continuum. The ionization and dissociation continuum are shown with respect to the absorption cross section in Figure 5.13.

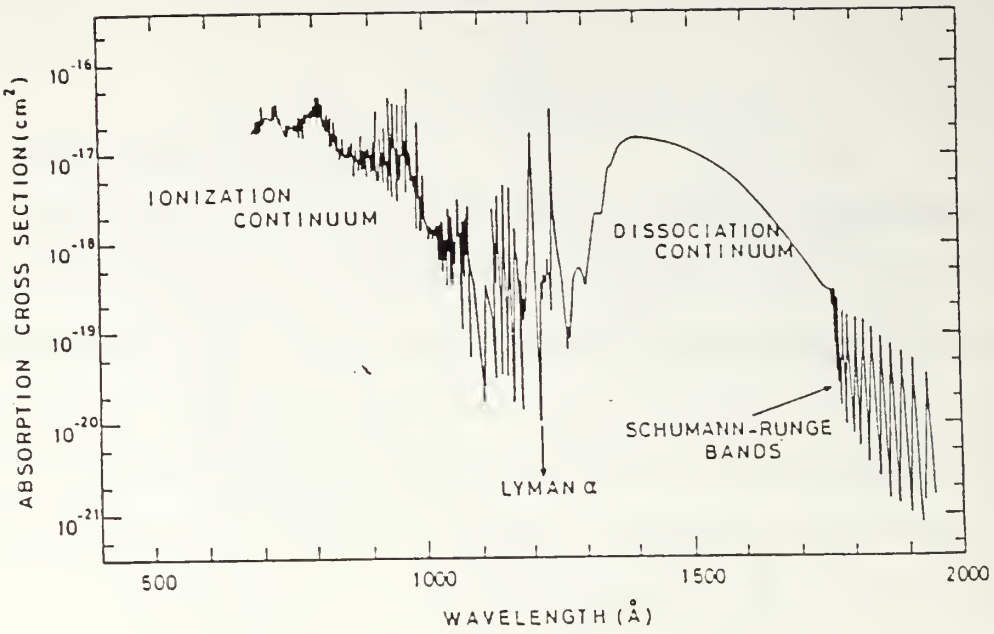

Figure 5.13 Absorption Cross-Section for O_2, Showing Continua, and SR Bands (Banks, and Kockarts, 1973)

For v' levels greater than three, the O_2 molecule will predissociate rather than fluoresce (Banks and Kockart, 1973). This means only the v'=0,1,2,3 states will contribute to the emission spectrum. In fact the Schumann-Runge system is actually the major source of atomic oxygen.

An estimate of the SR intensity can be made by comparing its g factor and the O_2 slant column density with the g factor and slant column density of known emissions. Barth (1965) lists the number of photons scattered per second per atom (g factors) for numerous atmospheric constituents. These g factors multiplied by the slant column density determine the relative strength of an allowed transition. The g factors for the first four v' states for the Schumann-Runge bands are extremely small. The largest value in the experimental wavelength range is 3.59×10^{-11} for the (3,7) band at 2442 Å. To put this in perspective a bright allowed feature such as the Nitric Oxide (1,0) gamma band, has a g factor of 7.7×10^{-6}. This implies that an NO Gamma transition is much more likely

than an O_2 Schumann-Runge transition. However, a contrasting value from Figure 2.08 shows that the number density for O_2 is about five orders of magnitude higher than NO. This would seem to imply that the strongest O_2 SR bands should be of comparable intensity to NO gamma bands. The values used to calculate the (3,7) SR band at an altitude of 150km for active solar conditions is provided in Table 5.03.

TABLE 5.03

O_2 $SR_{(3,7)}$ BAND INTENSITY CALCULATIONS

$g = 8.25 \times 10^{-9}$

$N = 1.8 \times 10^{18}$ mol cm^{-2} {for O_2 n(150km) = 1.0×10^9 mol cm^{-3}, t_{inf} = 1800°K, ch(30,90°)}

$4 \pi I = 4.2$kR

The Oxygen Schumann-Runge band system was not identified by Sharp (1986) in the thermosphere between 2000 and 8000 Å. No other experimental observation of this band has been found. However, it appears that emissions do exist in the experimental wavelength region, and they may contribute to the observed intensity.

The $^3\Sigma^-_u$ state is an allowed state for photon excitation from the $X^3\Sigma^-_g$ ground state. Once in the excited state the $^3\Sigma^-_u$ - to $^3\Sigma^-_g$ transition produces both P and R branches. Each branch has three components for a total of six main branches for each band. Additionally there are six satellite branches where $\Delta J \neq \Delta K$. Splitting will become significant only when K becomes large (Herzberg, 1950). The O_2 molecule has zero nuclear spin. This condition requires the molecule to follow Bose statistics (Herzberg, 1950). This requirement produces a band structure where every alternate triplet in the P and R branches appears. The band system is red degraded.

The synthetic spectrum for the SR bands that will fall in the window is shown in Figure 5.14. The synthetic spectrum shown is for all the v'=0,1,2,3. For v'>3 the molecule will predissociate rather than fluoresce.

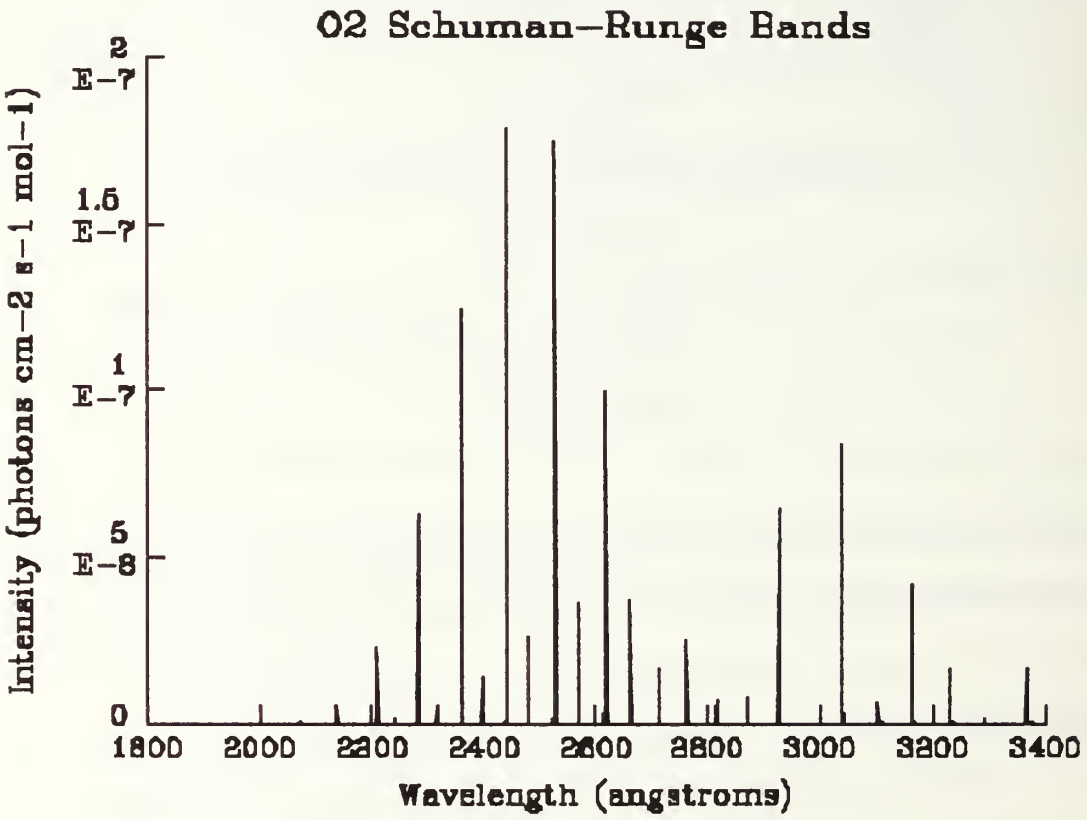

Figure 5.14 O_2 Schumann-Runge Bands

2. Herzberg Bands

The Herzberg transition ($A^3\Sigma^+_u$ - $X^3\Sigma^-_g$) appears to range from 2590 to 4880 Å (JPCRD, 1972). The band system appears to have been discovered rather recently by Herzberg, in 1952 (Pearse and Gaydon, 1963). The band system is a prominent feature in the nightglow, where the excitation source is inverse predissociation (Barth, 1965).

As a forbidden transition, Herzberg bands will result primarily from photoelectron impact. Its dayglow intensity will be less than a corresponding transition in the Schumann-Runge Band. The $\Sigma^+ \Leftrightarrow \Sigma^+$ or $\Sigma^- \Leftrightarrow \Sigma^-$ selection rule is the selection rule for this transition.

The upper state is subject to dissociation for incident energies greater than 5.1eV. It corresponds to a wavelength of 2420Å. This means that at any altitude, emissions as a result of the $A^3\Sigma^+_u$ - $X^3\Sigma^-_g$ transition will be longward of 2420 Å. The Herzberg dissociation peaks at 40 km and is closely linked with ozone production (Chamberlain, 1987). The $A^3\Sigma^+_u$ state dissociation reaction is shown below:

$$O_2 + e^*(E > 5.1eV) \Rightarrow O(^3P) + O(^3P) + e.$$

The calculation to determine the intensity of the Herzberg bands follows from that developed for the N_2 Second Positive bands. Figures 5.05, 5.06, and 5.07 are used to determine the intensity. The calculations were done for active solar conditions, looking across the limb. The brightest band identified is the (12,1) band at 2528Å. The factors used to determine the observed intensity are shown in Table 5.04.

TABLE 5.04

INTENSITY FACTORS FOR O_2(Herzberg)TRANSITION

$$\int_{E}^{E_{max}} \sigma_E I_E \, dE = 1.21 \times 10^{-7}$$

$q_{ov'\omega v'v''}$ (Q-omega) = 1.98×10^{-3} (Barth, 1965)

$N = 1.8 \times 10^{17}$ mol cm^{-2} {for O_2 n(150km) = 1.0×10^9 mol cm^{-3}, t_{inf} = 1800°K, ch(30,90°)}

$4 \pi I = 45R$

The calculated intensity of 45R is a marginal value as an observable value in the wavelength region. The Herzberg bands will contribute to the total observed intensity, however separate emission features may not be distinguishable. The O_2 Herzberg spectrum that contributes to the experimental window is shown in Figure 5.15.

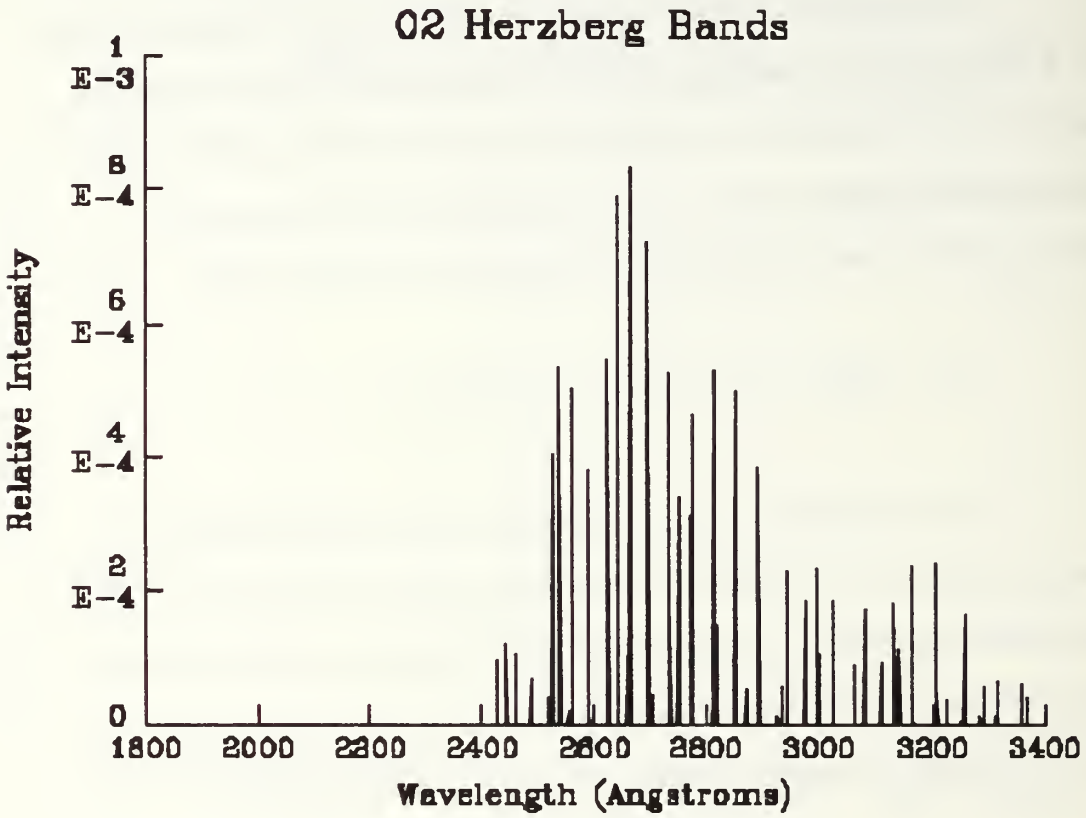

Figure 5.15 O_2 Herzberg Bands

C. NITRIC OXIDE

Nitric Oxide has three band systems in the experimental window. The Gamma band ($A^2\Sigma^+ - X^2\Pi$), Delta band ($C^2\Pi - X^2\Pi$), and Epsilon bands ($D^2\Sigma^+ - X^2\Pi$). The potential energy diagram for NO is shown in Figure 5.16. A schematic energy level diagram, which illustrates the major NO transitions, is shown in Figure 5.17.

Although NO has a significantly lower density compared with N_2, O_2, and O, the NO bands are very intense. As shown in Figure 2.08, at the lower end of the experimental altitude it is approximately five orders of magnitude less than the N_2 and O_2 densities. However, all of the the NO band systems are allowed transitions. The importance of nitric oxide as an emission source of the airglow becomes as significant as a corresponding forbidden transition of a more abundant species. The importance of NO diminishes with altitude beyond its peak number density at about 105 km. A fourth system, the Beta band ($B^2\Pi$ - $X^2\Pi$), also has transitions in the experimental window. However, the spatial overlap for this system results in intensities four to five orders of magnitude less than the other bands. It is not a significant contributor to the window.

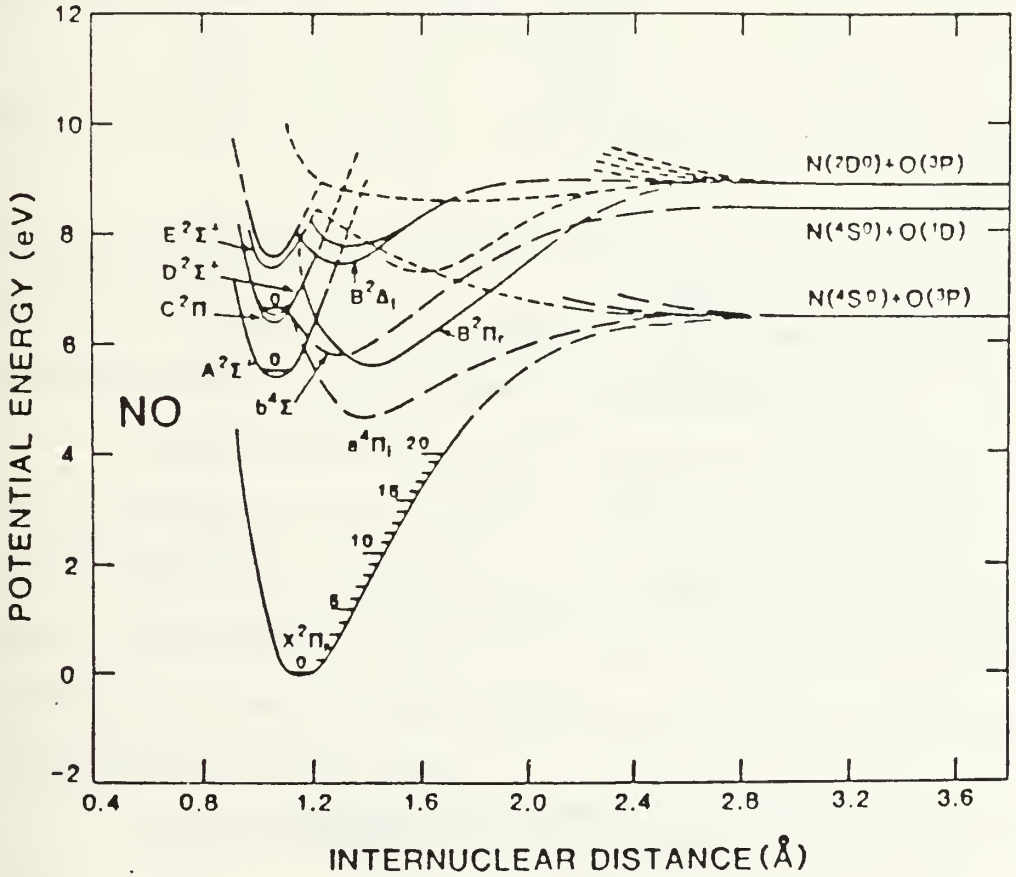

Figure 5.16 NO Potential Energy Diagram (Cleary, 1985)

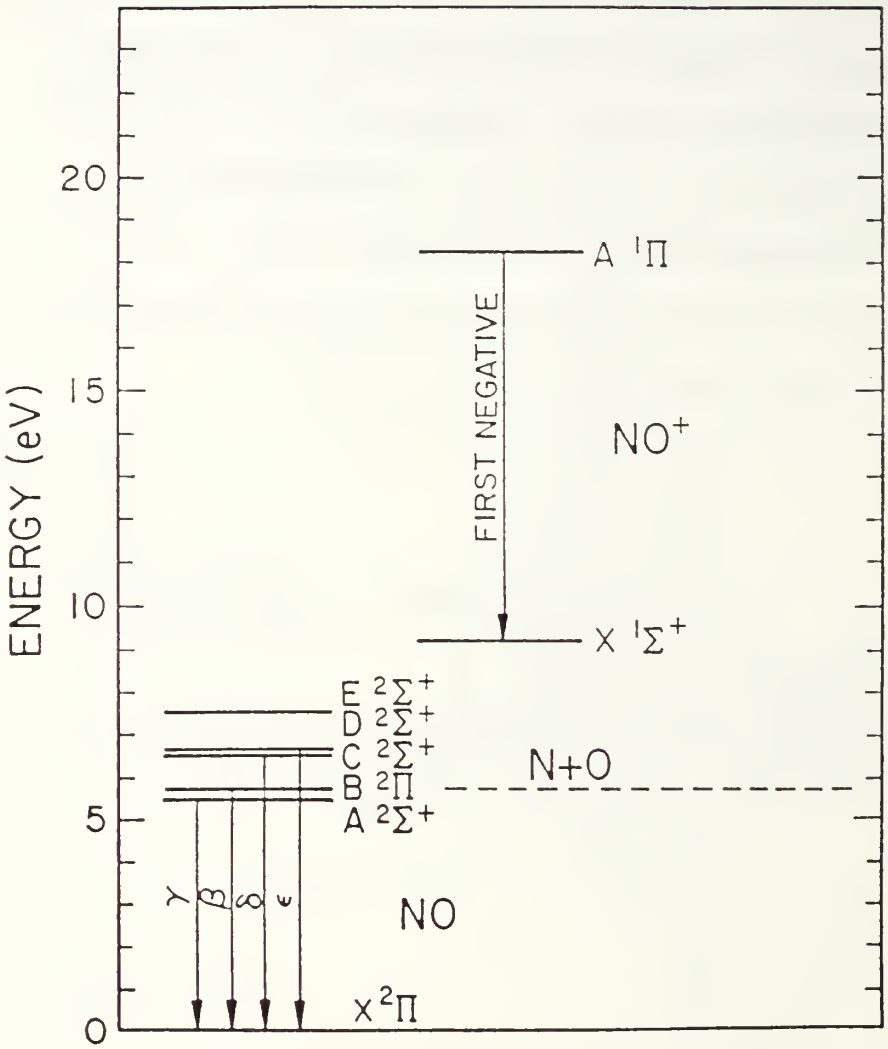

Figure 5.17 NO Energy Level Diagram

1. Gamma Band

The Gamma Band ($A^2\Sigma^+ - X^2\Pi$) is the most intense of the NO transitions in the experimental wavelength range. The bands range from 1873 to 6126 Å (Barth, 1965). The band system was observed as early as 1917 by Strutt (Pearse and Gaydon, 1963). It commonly occurs in flames containing nitric oxide as well as shock-treated air. The (1,0) Gamma band, at 2149 Å, is the most intense feature of Nitric Oxide in the ionosphere. The Gamma bands were not observed in the ionosphere until 1964 by Barth (1965).

The primary excitation mechanism for the upper state is photoexcitation. Other sources to the $A^2\Sigma^+$ state include cascade from the $C^2\Sigma^+$ state(Sharp, 1986) and the chemical reaction shown below:

$$NO(B^2\Pi;\ v=7) + M \Rightarrow NO(A^2\Sigma^+;\ v=3) + M \text{(Young \& Sharpless, 1962)}$$

These sources result in emission, where the NO molecule returns to the $X^2\Pi$ ground state . The upper state has a lifetime of $2x10^{-7}$ seconds (Callear and Pillings, 1970) which insures emissions rather than collisions will dominate activities in the state.

Measurements of the most intense Gamma bands are limited by self-absorption. Self-absorption has been observed by Cleary (1985) below 125 km for the (1,0) band at 2149Å, and below 115 km for the (2,0) band at 2047Å. These two bands are the strongest emission features of the gamma band system. Self-absorption is proportional to the column density times the oscillator strength for a band. This is why self-absorption is most significant for the strongest bands.

Nitric Oxide Gamma bands have been observed recently by Cleary (1986) in 1982, during active solar conditions. His observations yielded observed intensities of

about 30kR for the (1,0) band at an altitude of 105 km. This intensity had diminished to 2kR by an altitude of 190 km. Another measurement of the NO (1,0) gamma band at 2150 Å by Thomas (1978) was conducted during solar minimum conditions. His measurements indicate a measured slant intensity of 10 kR at 100 km, diminishing to less than 100R at 300 km. These figures support the prediction that the NO Gamma band will be a significant contributor to the experimental window, especially at low altitudes.

The upper state $A^2\Sigma^+$, conforms to Hund's case (b) while the ground state is an intermediate case of (a) and (b). The $^2\Sigma$ - $^2\Pi$ transition results in doublet splitting for both the upper and lower states. This produces a total of four band heads. Additionally, the $\Delta J = 0, \pm 1$ selection rule will result in P,Q, and R branches. Therefore the entire band will contain twelve branches. Bands are degraded to the blue (Herzberg, 1950). The emission spectrum of the NO Gamma band emission spectra is shown in Figure 5.18.

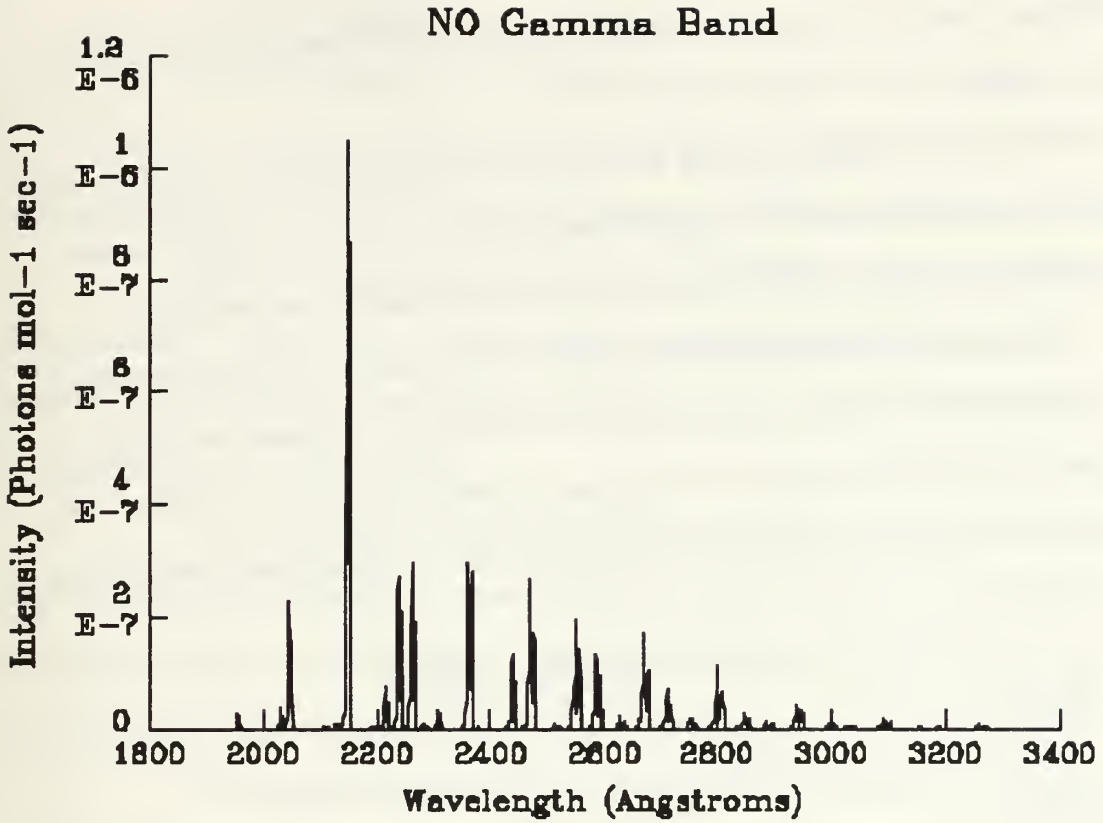

Figure 5.18 NO Gamma Bands (Cleary, 1985)

2. Epsilon Bands

The NO Epsilon bands ($D^2\Sigma^+$- $X^2\Pi$) are the same type of electronic transition, $^2\Sigma^+$- $^2\Pi$, as the gamma bands. The band system ranges appears to be most intense in the ultra-violet although precise wavelength ranges have not been identified. This emission system is one of the lesser known in the NO family, although it was observed by Guillery in 1927 (Pearse and Gaydon, 1963). Separate emission features in the ionosphere were identified by Cleary (1986).

The emission is a similar resonance scattering as the gamma bands. This means that an excitation from the ground state to the excited state leads to a relaxation back to the

ground state. The exclusive excitation mechanism for the $D^2\Sigma^+$ state is photoexcitation. (McCoy, 1981).

Cleary (1986) measured a peak intensity approaching 700 R/Å for the (0,1) band at 1950 Å at an altitude of 105 km. It appears that this band as well as the slightly weaker (0,2) at 2020Å and (0,3) at 2090Å features should be observable in the experiment.

Once again each band has four band heads, which yields the same twelve branch structure as the gamma bands. As shown in the potential energy diagram, an epsilon transition will be generally of higher energy than a corresponding gamma transition. The NO epsilon bands that will contribute to the experimental wavelength region are shown in Figure 5.19.

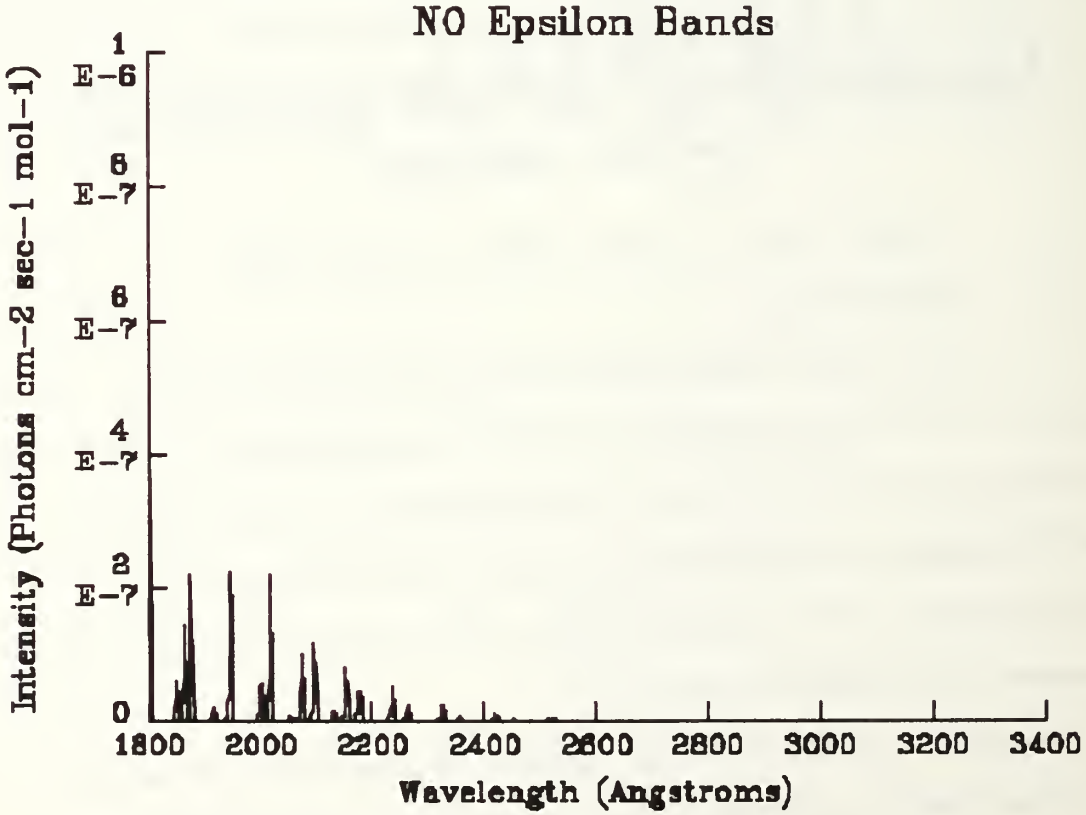

Figure 5.19 NO Epsilon Bands (Cleary, 1985)

3. NO Delta Bands

The Delta Bands ($C^2\Pi - X^2\Pi$) are also an allowed transition for the $^2\Pi - {}^2\Pi$ case. Delta bands range from 1621 to 4288 Å. Early observations of this band system were made by Knauss in 1928, and Schmid in 1930 (Pearse and Gaydon, 1963).

The Delta excitation mechanism is photoexcitation similar to the Epsilon and Gamma bands. Delta bands do not demonstrate a fluorescence efficiency of unity, however. The accepted efficiency factor is .25 (Cleary 1986). This low efficiency is required because of predissociation.

Cleary (1986) also observed delta bands during his 1982 experiment . Sharp (1986) has not identified any more recent observations. The strongest feature observed by Cleary was the (0,1) band at 1980 Å. He measured a peak intensity of about 150 R/Å which will be difficult to distinguish in the experimental wavelength region.

Once again each band has four band heads, which yields the same twelve branch structure as the gamma bands. As shown in the potential energy diagram, a delta transition will be generally of higher energy than a corresponding gamma transition, although it is of a slightly lower energy than the epsilon bands. The NO delta bands that will contribute to the experimental wavelength region are shown in Figure 5.20.

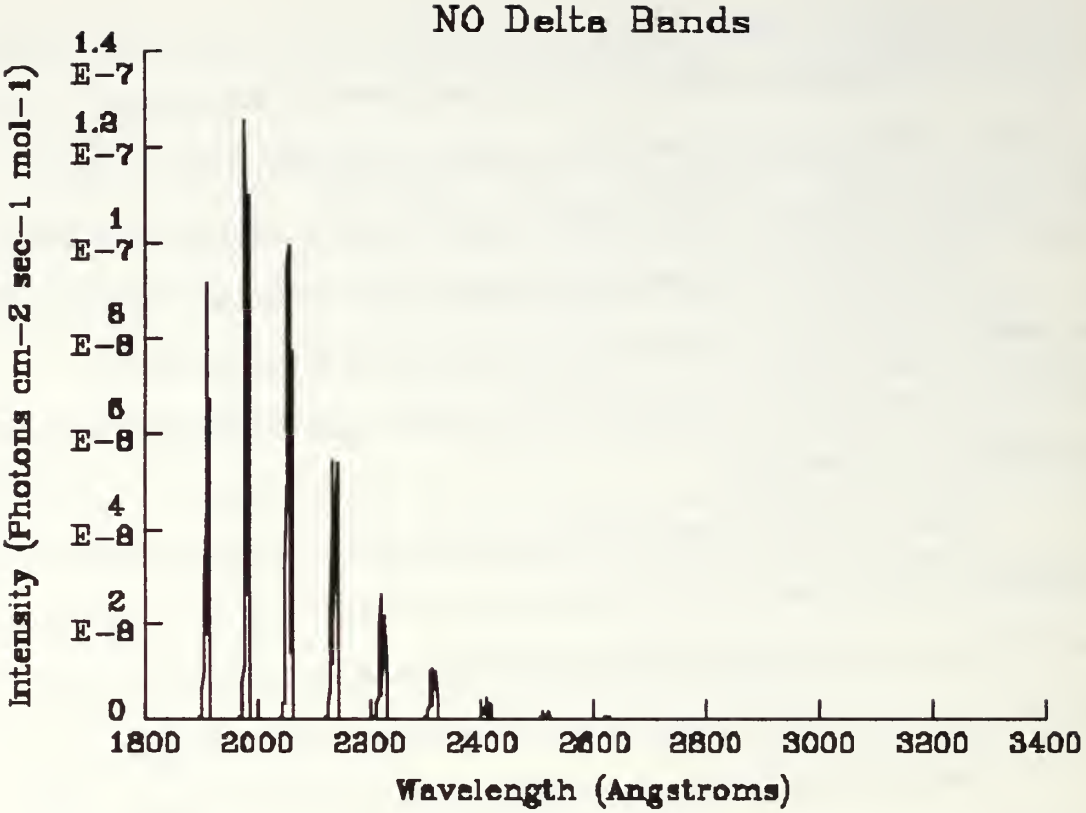

Figure 5.20 NO Delta Bands (Cleary, 1985)

D. ATOMIC OXYGEN

There is one atomic oxygen line that occurs in the experimental window. This is the 2972 Å line. The line is a result of the ($O(^1S)$ - $O(^3P)$) transition. It is a well known forbidden emission of the oxygen atom.

This line is represented by the transition shown below.

$$O(^1S) \Rightarrow O(^3P) + h\upsilon(2972\text{Å})$$

This transition is forbidden as it violates $\Delta S = 0$ requirement for atomic transitions. Although forbidden, this transition has been reported by Sharp at an average intensity of 80R. This is a marginal observed intensity. Furthermore, this line is near the 3000Å instrument efficiency cutoff which will tend to further limit the observed intensity. However, the relative density rises steadily throughout the experimental altitude range. The 2972Å line will be swamped by stronger emissions at low altitudes in the experimental region but could be distinguishable at higher altitudes. This will be especially true when O becomes the dominant constituent above 175 km.

The upper state for this transition, the O(^{1}S) state, is the source of two branches. These two branches are shown in the energy level diagram of Figure 5.21.

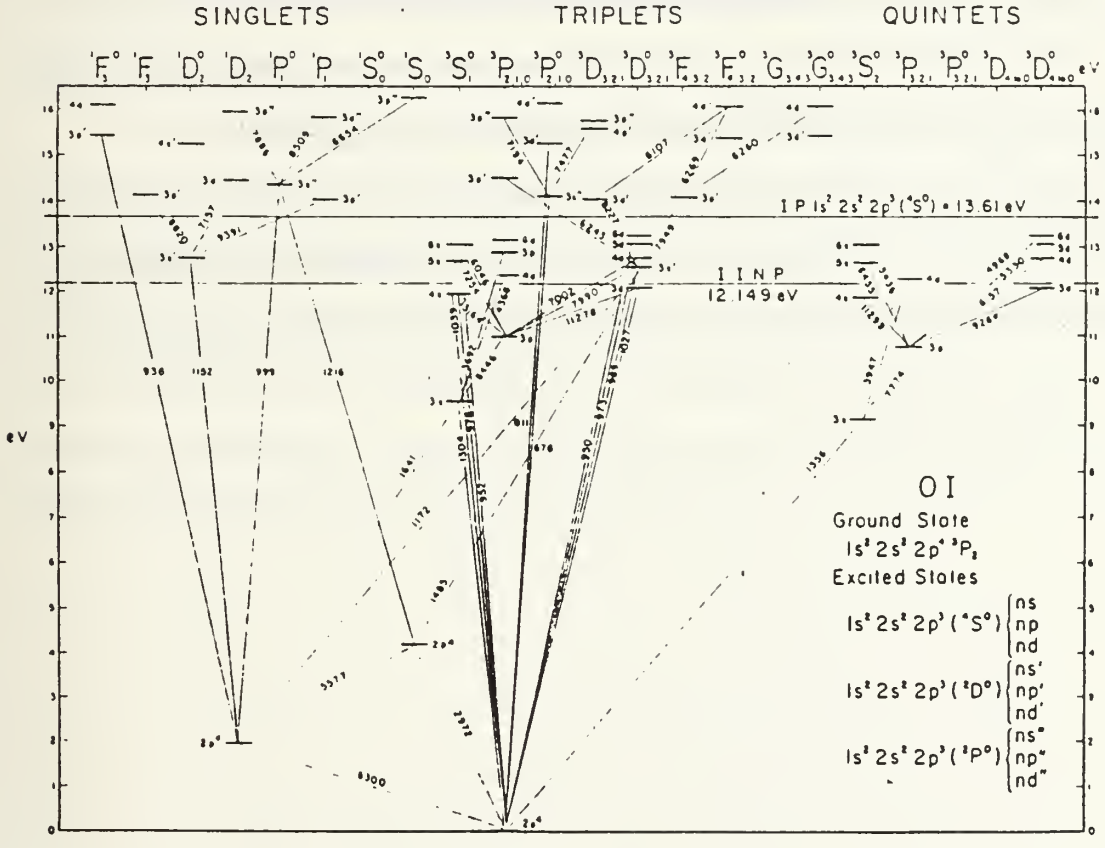

Figure 5.21 O Energy Level Diagram

It is clear from Figure 5.21 that an O atom in the ^1S state can either emit a 2972 or 5577 Å photon. Furthermore, since the branching ratio between the 5577 and 2972 Å lines has been determined a measurement of the 2972Å feature can be used to determine source terms for the O(^1S) state. The sources for the O(^1S) state are shown in Table 5.05.

TABLE 5.05

OXYGEN (^1S) SOURCES

$O + e$

$O_2^+ + e^*$

$O_2^+ + N$

$N_2(A^3\Sigma_u^+) + O$

These sources include N_2 in the upper state for Vegard-Kaplan bands. This relationship could be used to assist in determining the quenching rate for the $A^3\Sigma^+_u$ state of N_2. Cross-sections and efficiencies for these source terms are given by Sharps (1986).

The 2972 Å line should be observable in the experimental window. It is near the limit of optimum detector efficiency, but below the 3000 Å threshold of reduced efficiency. It appears that this line may also be useful in determining N_2 molecular densities as well.

VI. CONCLUSION

A. SUMMARY OF FINDINGS

Identification of emissions in the wavelength range of the MUSTANG experiment was accomplished using experimental results to support calculated emission feature intensity. All emission bands that will contribute to the experimental spectrum, as well as those features that will be distinguishable, have been tentatively identified. These results confirm the contention that the instrument wavelength range allows observation of all midultraviolet airglow emission bands. The extended wavelength and altitude range for this experiment allows a unique experimental opportunity to observe all major neutral atmospheric constituents in one spectrum.

The major midultraviolet emission bands are shown in Table 6.01. This table also identifies the brightest emission feature, its wavelength, and whether or not the band will be distinguishable. The last column provides special circumstances for observations of that band system. This column considers the most intense feature and accounts for the 3000Å instrument efficiency cutoff, where appropriate. It can be seen in Table 6.01 that the spectrum is quite complex. Analysis of experimental results will require unfolding each constituent spectrum from the combined observed spectra.

TABLE 6.01

MUSTANG EXPERIMENT: OBSERVABLE EMISSIONS

Species	System	Band	λ (Å)	Observable
N_2	VK	(5,1)	1841	above 200km
	2P	(2,0)	2973	marginal due low Q-ω
		(1,0)	3157	marginal due to inst. eff
	LBH	(3,9)	1854	yes
O_2	SR	(3,7)	2442	yes
	H-I	(12,1)	2528	marginal
NO	γ	(1,0)	2149	yes
	ε	(0,1)	1950	yes
	δ	(0,1)	1980	marginal
O	line	N/A	2972	above 175km

B. TOPICS FOR FURTHER INVESTIGATION

This preliminary identification of the predicted experimental spectrum for the MUSTANG experiment must initially be confirmed by data analysis to identify those emission features in Table 6.01. This data will then be analyzed to identify N_2 density in the E, F1, and F2 regions along with NO density in the E region. Further analysis along with data from the HIRAAS instrument will be used to identify the solar EUV flux and photoelectron flux. These results will contribute significantly towards meeting the DOD goal of identifying the ionospheric electron density. The experimental wavelength range allows observation of all major neutral contributors and a self consistent model of the electron density may be possible when analysis of all experimental results is complete.

BIBLIOGRAPHY

Ahmed, M., "N_2 Vegard-Kaplan Band System in Aurora: Rotational Temperatures and Vibrational Populations," *Journal Atmospheric and Terrestrial. Physics, 31*, 1259, 1969.

Banks, P.M. and Kockarts, G., *Aeronomy*, Academic Press, Inc., 1987.

Barth, Charles A., "Rocket Measurement of Nitric Oxide in the Upper Atmosphere," *Planetary Space Science., 14*, 623,1966.

Barth, Charles A., "Ultraviolet Spectroscopy of Planets," *Jet Propulsion Lab Technical Report No. 32-822*, 1965.

Borst, W.L., "Excitation of Several Important Metastable States of N_2 by Electron Impact," *Physics Review., 5*, 648, 1972.

Brigham, E. Oran, *The Fast Fourier Transform and its Applications*, Prentice-Hall, Inc., 1988.

Broadfoot, A.L. and Hunten, D.L., "Excitation of N_2 Band Systems in Aurora," *Canadien Journal of Physics, 42*, 1212, 1964.

Callear, A.B, and Pilling, M.J., Fluorescence of Nitric Oxide, Part 6: Pred. of D.C. states; oscillator strengths δ_{oo}, ε_{oo}, part 7: Quenching Rates of C and rad to A state,"*Faraday Society., 66*, Part 6, 1886, Part 7: 1618, 1970.

Campbell, I.M., and Thrush, B.A., "The Recombination of Nitrogen Atoms and the Nitrogen Afterglow," *Procedures of the Research Society of London, Serial A, 296*, 201, 1967.

Cartwright, D.C., Trajmar, S., Chutjian, A., Williams, W.,"Electron Impact Excitation of the Electronic States of N_2, II. Integral Cross Sections at Incident Energies from 10 to 50 eV," *Physics Research, 1041*, 1977.

Chamberlain, Joeseph W., *Theory of Planetary Atmospheres*, Second Edition, Academic Press, Inc., 1987.

Cleary, D.D., *Analysis of Nitric Oxide Fluorescence Bands from High Latitude Rocket Observations of the Thermospheric Dayglow*, Ph.D Dissertation, University of Colorado, 1985.

Cleary, D.D., "Daytime High-Latitude Rocket Observations of the NO γ, δ, and ε Bands," *Journal of Geophysical Research*, 94, 11337, 1986.

Conway, R.R.,"Self-Absorption of the N_2 Lyman-Birge-Hopfield Bands in the Far Ultraviolet Dayglow, *Journal of Geophysical Research, 87 No. A2*, 859, 1982.

Conway, R.R., *Spectroscopy of the Mars Airglow from Mariner 9 Ultraviolet Spectrometer Data*, Ph.D. Dissertation, University of Colorado, 1980.

Conway, R.R., and Christensen, A.B., "The Ultraviolet Airglow at Solar Maximum 2. Solar Photometer Observations of N_2 Second Positive (0,0) Band Emission," *Journal of Geophysical Research, 89 No. A7*, 6601, 1985.

Earls, L.T., "Intensities in $^2\Pi$-$^2\Sigma$ Transitions in Diatomic molecules," *Physical Review*, 48, 423, 1935.

Eccles, M.J., *Low Light Level Detectors in Astronomy*, Cambridge University Press, 1983.

Eisberg, R., and Resnick, R., *Quantum Physics of Atoms, Molecules, Solids, Nuclei, and Particles*, Second Edition, John Wiley & Sons, Inc., 1985.

Fastie, William G. "A Small Plane Grating Monochromator," *Journal of the Optical Society of America, 42 No.9*, 641, 1952.

Gilmore, F.R., "Potential Energy Curves for N_2, NO, O_2, and Corresponding Ions," *Journal of Quantitative Spectroscopy and Radiative Transfer*, 5, 369, 1965.

Hecht, Eugene, *Optics*, Addison-Wesley Publishing Co., 1987.

Hedin, A.E., "A Revised Thermospheric Model Based on Mass Spectrometer and Incoherent Scatter Data: MSIS-83," *Journal of Geophysical Research*, 88, 10170, 1983.

Herzberg, G., *Atomic Spectra and Atomic Structure*, Dover Publications, 1944.

Herzberg, G., *Molecular Spectra and Molecular Structure I. Spectra of Diatomic Molecules*, D. Van Nostrand Reinhold Company, 1950.

Huber, K.P., and Herzberg, G., *Molecular Spectra and Molecular Structure IV. Constants of Diatomic Molecules*, Van Nostrand Reinhold Company, 1979.

Hund, F., "Zur Deutung der Molekulspektren. II," *Zeitschrift Physik, 42*, 93, 1927.

Krupenie, Paul H.and Lofthus, Alf, "The Spectrum of Molecular Nitrogen," *Journal of Physical Chemistry Reference Data, 6 No. 1*, 139, 1977.

Krupenie, Paul H., "The Spectrum of Molecular Oxygen," *Journal of Physics and Chemist ry Reference Data, 1 No. 2*, 433, 1972.

Massie, S.T., "Nitric Oxide Band Absorption Measurement in the Lower Thermosphere," *Journal of Geophysical Research, 85 No. A5*, 2155, 1980.

McCoy, R. P., *Rocket Measurements of Thermospheric Odd Nitrogen and Comparisons with a Diffusive Transport Chemical Model*, Ph.D. Dissertation, University of Colorado,1981.

NASA Technical Report 32-822, *Ultraviolet Spectroscopy of Planets*, C.A. Barth, 1965.

Oran, E.S. and Strickland D.J., "Photoelectron Flux in the Earth's Ionosphere," *Planetary Space Science, 26*, 1161, 1978.

Pearse, Jeffrey P., *Rocket Measurement of Nitric Oxide in the Earths Atmosphere Between 60 and 96 Kilometers*,Ph.D. Dissertation, University of Colorado, 1968.

Pearse, R.W.B. and Gaydon, A.G., *The Identification of Molecular Spectra*, Chapman and Hall LTD, 1963.

Research Support Instruments Inc., *Array Detector Assembly (with Intensifier)* - Drawing, 31 October 1989.

Samson, James A., *Techniques of Vacuum Ultraviolet Spectroscopy*, Pied Publications, 1967.

Sawyer, Ralph A., *Experimental Spectroscopy*, Second Edition, Prentice-Hall, 1951.

Sharp, William Edward, *Rocket-Borne Spectroscopic Measurements of the Nitrogen Vegard-Kaplan Bands in the Ultraviolet Aurora*, Ph.D. Dissertation, University of Colorado, 1970.

Siskind, D.E., and Barth, C.A., "Rocket Observations of the NII 2143Å Emission in Aurora," *Geophysical Research Letters, 14*, 479, 1987.

Sharp, William Edward, "Chemiluminescence of Nitric Oxide: the NO ($C^2\Pi$-$A^2\Sigma^+$) Rate Constant," *Journal Quantitative Spectroscopy. Radiative Transfer, 25*, 413, 1981.

Sharp, William Edward, "Sources of the Emission Features Between 2000 and 8000Å in the Thermosphere," *Canadian Journal of Physics, 64*, 1594, 1986.

Shemansky, D.E. and Broadfoot, A.L., "Excitation of N_2 and N_2^+ Systems by Electrons, I Absolute Transition Probabilities," *Journal of Quantitative Spectroscopy and Radiative Transfer, 11*, 1401, 1971.

Strickland, D.J. and Meier, R.R., "A Photoelectron Model for the Rapid Computation of Atmospheric Excitation Rates," *NRL Memorandum Report 5004*, 1982.

Strobel, D.F., Oran, E. and Feldman, P.D., "The Aeronomy of Odd Nitrogen in the Thermosphere 2. Twilight Emissions," *The American Geophysics Union, 81 No. 22*, 3745, 1976.

Tascione, T.F., *Introduction to the Space Environment*, Orbit Book Company, Inc. 1988.

Tatum, J.B., "The Interpretation of Intensities in Diatomic Molecular Spectra," *The Astrophysical Journal Supplement Series, 14*, 21, 1967.

Thomas, Ronald J., "A High-Altitude Rocket Measurement of Nitric Oxide," *Journal of Geophysical Research, 83 No. A2*, 513, 1978.

Torr, M.R. and Torr, M.R., "The Role of Metastable Species in the Thermosphere," *Reviews of Geophysics and Space Physics*, 20 No.1, 91, 1982.

Torr, M.R. and Torr, M.R., "Ionization Frequencies for Major Thermospheric Constituents as Functions of the Solar Cycle," *Geophysical Research Letters, 6 No. 10*, 771, 1979.

Young, R.A. and Sharpless, R.L., "Discussion," *Faraday Society 33*, 228, 1962.

INITIAL DISTRIBUTION LIST

		No. Copies
1.	Defense Technical Information Center Cameron Station Alexandria, Virginia 22394-6145	2
2.	Library, Code 0142 Naval Postgraduate School Monterey, California 93943-5002	2
3.	Dr. K.E. Woehler, Chairman 61 Physics Department Naval Postgraduate School Monterey, California 93943-5000	1
4.	Dr. D. D. Cleary Physics Department 61-Cl Naval Postgraduate School Monterey, California 93943-5000	5
5.	Dr. S. Gnanalingam Physics Department 61-Gm Naval Postgraduate School Monterey, California 93943-5000	1
6.	CPT Gary M. Danczyk LANL MS-M997 Los Alamos New Mexico 87545	2

Thesis
D14756 Danczyk
c.1 Identification of thermospheric dayglow spectrum for the MUSTANG experiment.